An analysis of the consistency between observed atmospheric winter variability and weather anomalies in the North Atlantic region

Master Thesis

MSc *Climate Change*

Simon Peter Heselschwerdt

Supervisor: Jens Hesselbjerg Christensen

May 2022

University of Copenhagen

Faculty of Science

Niels Bohr Institute - Physics of Ice, Climate and Earth (PICE)

Acknowledgments

I would like to thank my thesis supervisor Jens Hesselbjerg Christensen of Physics of Ice, Climate, and Earth at the University of Copenhagen, for his wise and valuable advice during my research. Thanks for letting me participate in interesting meetings with other researchers and guiding me through the whole process. Furthermore, I would like to thank Anna Kirchner, whose Master thesis covers similar aspects as my analysis but with a particular focus on climate models. Her work is a complementing approach to my work, and, hence, she helped me with valuable discussions and coding tips. Also, I would like to thank Celine Strufe for proofreading my drafts and giving me valuable hints in structuring my thesis. Lastly, my sincere gratitude goes to all my family and friends for supporting me throughout this two-year experience full of academic and personal lessons.

Abstract

The complex spatial and temporal evolution of large-scale atmospheric circulation in the North Atlantic region is simplified by modes of climate variability. Those modes of variability present a pronounced teleconnection with weather conditions in the area, posing a high significance for present climate science. Hence, this thesis aims to analyze the relationship between observed atmospheric winter climate variability and temperature and precipitation anomalies. Therefore, an empirical orthogonal function analysis of mean sea level pressure in the North Atlantic region for the period 1950-2021 has been conducted. In doing so, the ERA5 reanalysis dataset has been used to analyze atmospheric modes of variability during the extended boreal winter season (NDJFM). Additionally, a principal component regression analysis has been performed to examine the importance of the different climatic modes on weather conditions, with a particular focus on more extreme anomalous winter conditions. The empirical evidence in this dissertation confirms a strong influence of the climatic modes on the weather conditions in the North Atlantic domain. Although the NAO is generally identified as the governing variability mode, the findings of this paper outline an unexpected asymmetry of the NAO pattern with respect to the temperature segregated analyses. Besides, this study demonstrates characteristic teleconnection patterns of the four leading variability modes. The stated findings may be considered a promising aspect of reconstruction approaches, particularly in the scope of the GreenPlanning project.

Keywords: ERA5 reanalysis, atmospheric modes of variability, NAO, climate variability, NAO reconstructions, empirical orthogonal function analysis, principal component regression analysis, GreenPlanning project

Contents

List of Figures

List of Tables

Abbreviations

C3S - Copernicus Climate Change Service
CDS - C3S Climate Data Store
ECMWF - European Centre of Medium-Range Weather Forecasts
EOF – empirical orthogonal function
ERA5 BE - ERA5 back extension
GP500 – geopotential height at 500 hPa
IFS - Integrated Forecast System
MSLP – mean sea level pressure
NAO – North Atlantic Oscillation
NDJFM – November, December, January, February, March
PC - principal component
PCR - principal component regression
PCs – principal component time series
TAS – two-meter temperature
TP – total precipitation

1 Introduction

Climate change has been increasingly perceived as a critical challenge to human society (Edenhofer et al., 2014). Therefore, a profound understanding of the climate system and its variability is crucial in terms of expedient adaptation and mitigation measurements.
Complex interactions between the different components of the earth system (atmo-, lito-, cryo-, hydro-, and biosphere) define variations in the mean state of the climate system (Goosse, 2015). Here, the diverse processes take place at different timescales and contribute in various ways to the variability of the system (Mitchell, 1976). The potential drivers of climate variability are internal processes (e.g., interactions within the system), as well as external forcings (e.g., orbital parameters). Recurring spatial patterns of climate variability and their fluctuations across different timescales can be referred to as modes of climate variability (Stephenson et al., 2004).
In previous research, statistical analyses of observational or model data have been used to identify different modes of variability. These modes are described by a characteristic spatial pattern and its associated time series (Christensen et al., 2013). However, to some extent, the defined modes are elements of the statistical analysis approach itself. Hence, they constitute a background state of the weather on timescales of a season's or years' rather than a definite synoptic scale. In this regard, modes of climate variability represent a simplification of the climate system's complex spatial and temporal evolution (Hernández et al., 2020).
The atmospheric circulation variability in the North Atlantic region dictates the prevailing weather conditions in that area, particularly in boreal winter. Furthermore, influences on ocean properties and ecologic systems have been claimed (Hurrell and Deser, 2010). Concerning this matter, recent studies focused on the most prominent and recurrent pattern, the North Atlantic Oscillation (NAO) (Hurrell et al., 2003). Remarkably, an unusually positive NAO phase was related to the extreme heatwaves in the summer of 2003 that were recorded in large regions of the European region (Beniston, 2004). Hence, understanding the different modes of variability and their relationship with temperature and precipitation anomalies poses a crucial component in current climate science. However, the interrelationships of the dominant variability modes and weather conditions are still debated, particularly under on more extreme anomalous winter conditions. Besides, more robust understandings of these correlations are crucial in terms of reconstruction approaches of the atmospheric variability, e.g., in the scope of the *GreenPlanning* project.
Therefore, this study analyzes the hypothesis *that certain modes of variability dominate climate variability in the boreal winter season.* Additionally, this paper explores the related research question of *whether and to what extent these modes have a profound correlation to climatic conditions in certain areas of the North Atlantic domain.* The analysis focuses on the extended winter season mean from November to March (NDJFM), as climate variability is most pronounced during this

time of the year. Moreover, an unprecedented approach will be carried out addressing modes of variability and their influence on climate conditions for more extreme anomalous winter seasons in the Northern European region. This is of particular interest for reconstruction approaches as proxy data rather reflect extremer periods than the norm.

The thesis is structured as follows: First, section 2 presents an overview about atmospheric modes of variability in the North Atlantic Region and its reconstruction. Then, section 3 introduces the used data of the *ERA5* reanalysis product and summarizes the performed data preprocessing and the methodological approach. The following section 4 presents the results of the (4.1) *empirical orthogonal function* (*EOF*) analysis and the (4.2) *principal component regression* (*PCR*) analysis of the winter mean sea level pressure for the period 1950-2021 and, separately, (4.3) for years with extreme anomalous temperature and precipitation conditions in the Northern Europe. Section 5 discusses the findings, their limitations and future work. Lastly, section 6 provides a conclusion of the thesis.

2 Climate Variability

2.1 Atmospheric Modes of Variability in the North Atlantic Region

Atmospheric variability in the North Atlantic region is of crucial importance for the prevailing climatic conditions. According to Hurrell (1995), the intra-seasonal to decadal variability is dominated by the *NAO*. This mode of climate variability is defined by the sea level pressure difference between the subtropical high and subpolar low (Hurrell et al., 2003). However, the *NAO* pattern is present across the entire troposphere as a virtually consistent pattern (Wanner et al., 2001). The centers of action are of reverse polarity and situated in proximity to Iceland and the Azores (figure 2.1). The sea level pressure gradient oscillates without a periodical pattern between a positive *NAO*, defined by a large pressure gradient, and a negative *NAO*, characterized by a smaller pressure gradient (Schmith et al., 2022). A useful approximation describing the atmospheric modes is the *NAO* Index, presenting the prevailing pressure gradient between the two centers of action. Still, a more robust alternative is the principal component time series (*PCs*) of the leading *EOF* of the sea level pressure in the North-Atlantic region (Lehner et al., 2012).
The *NAO* substantially influences other dynamical climatological features over the North Atlantic and adjacent continents. The effects are more significant in boreal winter when the *NAO* explains more than one-third of the sea level pressure variance (Hurrell et al., 2003). Variations of the sea level pressure gradient affect the westerlies' mean strength and thus also change the advection pattern of air masses (Schmith et al., 2022). Consequently, prevailing weather conditions over Europe change (Hurrell et al., 2003). An analysis by Kenyon Hegerl (2008) regarding temperature extremes over Eurasia has shown a pronounced continent-wide effect of the *NAO*. Affecting not only the mean temperature but also extremes emphasize the cruciality of the *NAO* as a driver for climate extremes, hence, its importance for climate change adaptation.
Another study by Haylock *et al.* (2004) determined the significant impact of the *NAO* on extreme winter rainfall by analyzing observations of 347 European meteorological stations for the period 1958 to 2000. The results, furthermore, emphasize contrasting effects of the two NAO modes on precipitation with a divide between northwestern Europe and the Mediterranean (Hurrell and Deser, 2010).
The impacts of different *NAO* states can be seen in figure 2.1. A strong pressure gradient (*NAO+*) leads to pronounced westerlies during the winter months, transporting warm and humid air from the ocean to Northern Europe. In contrast, a weaker pressure gradient (*NAO-*) leads to a more wobbly north-south air movement, accompanied by cold and dry winter weather in Northern Europe. Another bipolar pattern of the *NAO* can be seen between Northern Europe and Greenland (Davini et al., 2012). Here, a positive *NAO* leads to northerly arctic winds and cold conditions

over Greenland. In contrast, a negative *NAO* implies a more frequent transition of low-pressure systems, a westward movement of the subpolar gyre, and a warming of the Atlantic current traveling clockwise around Greenland (Häkkinen and Rhines, 2004). These complex effects of the different *NAO* states affect, besides temperature and precipitation, various other climatological components, e.g., the sea surface temperature, sea ice occurrence, and further ocean characteristics (Hurrell and Deser, 2010).

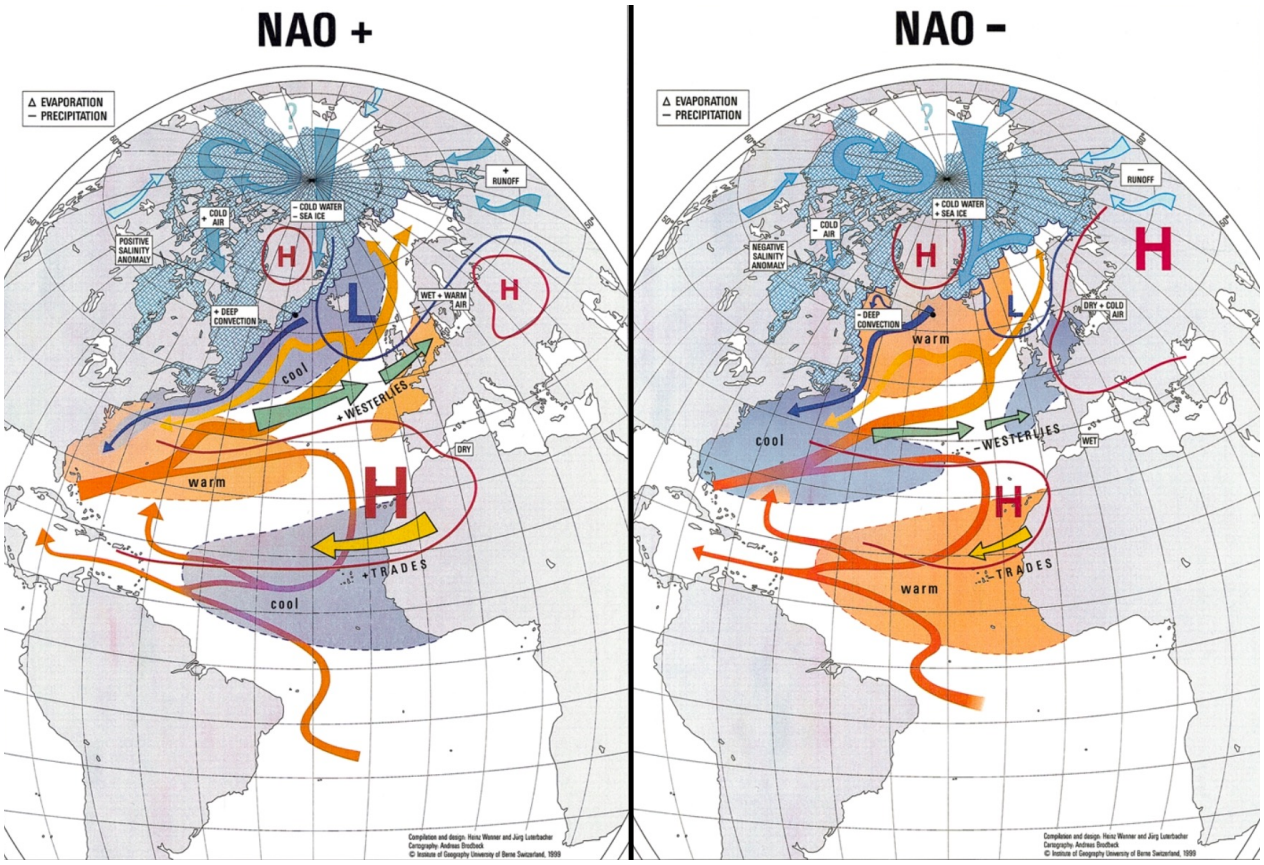

Figure 2.1: The two phases of *NAO* and their impacts on weather conditions at the North Atlantic region. Taken from Wanner *et al.* (2001).

Frequently associated with the respective modes of climate variability are nearly stationary high-pressure systems. These blocking highs usually occur on synoptic timescales of more than one week and influence the eastward migration of weather systems over the North Atlantic (Ruggieri et al., 2020). Regarding this, Shabbar *et al.* (2001) stated that winters with a predominant positive *NAO* correlate with substantially more blocking episodes over the North Atlantic than winters dominated by a negative *NAO*. Consequently, prolonged and consistent weather conditions appear while the risk for extreme events increases. For instance, the extreme heatwaves over Europe in the summer of 2003 or 2018 were linked to a positive *NAO* phase (Trigo et al., 2005; Drouard et al., 2019). Negative *NAO* states often correlate with blocking highs over Greenland (*Greenland*

Blocking). Other appearing blocking situations are the *Scandinavian Blocking* and the *Atlantic Ridge Blocking*, which are associated with different modes of interannual climate variability and are defined by characteristic spatial patterns of pressure systems (figure 2.2). All modes of atmospheric variability pose a link between climate conditions in different areas of the North Atlantic region (Ruggieri et al., 2020).

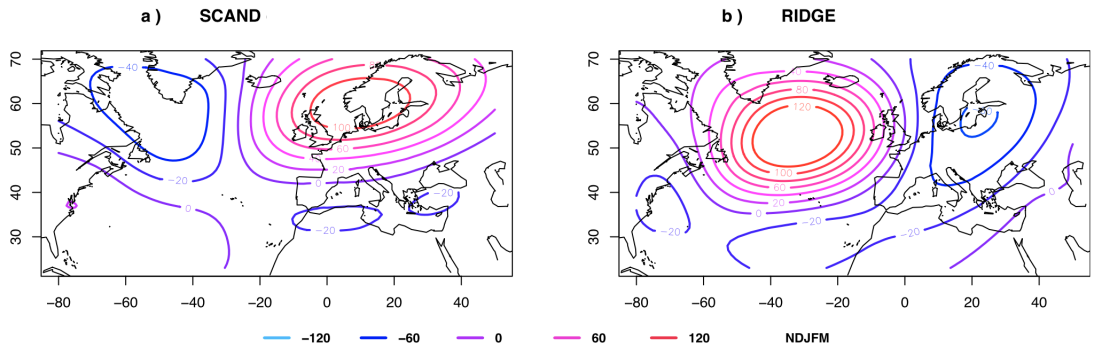

Figure 2.2: a) *Scandinavian Blocking* and b) *Atlantic Ridge Blocking*. Contours indicate anomalies of geopotential height at 500 hPa [m] for the extended cold season in ERA-Interim. Taken from Ruggeri *et al.* (2020).

The atmospheric circulation variability is mainly driven by non-linear dynamics of the extratropical atmosphere, with the dominating mechanism being interactions between the time-mean flow and synoptic timescale transient eddies (Ruggieri et al., 2020). Therefore, the phase's trajectory and amplitude of the *NAO* on a monthly or even annual scale seemed to be largely unpredictable (Hurrell and Deser, 2010). However, Schmith *et al.* (2022) determined that the preceding *NAO*-index values affect the strength and spatial pattern of the following *NAO* event (preconditioning). Furthermore, this preconditioning influences associated circulation features, precipitation, and temperature patterns. Studies by Smith *et al.* (2020) and Athanasiadis *et al.* (2020) have demonstrated the prediction of the prevailing phases of the *NAO* dominating seasonally and the North Atlantic atmospheric blocking several years ahead. However, the underlying mechanisms are still not fully discovered. Due to the significant impact of the North Atlantic atmospheric variability on the climatic circumstances and the livelihood of the surrounding continents, more reliable predictions and a more profound understanding are crucial steps for effective climate change adaptation (Hurrell and Deser, 2010).

2.2 Reconstruction of the North Atlantic Atmospheric Variability

The significant influence of the North Atlantic atmospheric variability underlines the urgency for a comprehensive understanding of the underlying mechanisms. However, the measurement and avail-

ability of the relevant climatic variables cover merely the last centuries. Extended climate records, reaching beyond the era of instrumental measurements, are crucial for a sufficient understanding of the complex interactions (Hernández et al., 2020). Hence, applying indirect climate indicators (proxies) from various archives, e.g., ice cores, lake sediments, or tree rings, is of paramount importance (Neukom et al., 2019).

Proxy-based records comprise information about prevailing environmental conditions such as temperature and precipitation. The teleconnection between these climate variables and atmospheric circulation enables an approach to reconstructing past climatic variability (Bradley, 2015). In this regard, a variety of studies have utilized this interrelationship to reconstruct atmospheric variability for a wide range of timescales and temporal resolutions (e.g., Vinther et al., 2003; Ortega et al., 2015; Becker et al., 2020 and others).

Nevertheless, the reliability of the reconstructions is limited as, e.g., the the proxies' characteristics influence the results. Identifying locations with a significant relationship between the proxy-related climatic variable (e.g., temperature or precipitation) and the respective atmospheric mode of variability constitutes a more robust reconstruction. Concerning this matter, a stable relationship between the proxy signal and the atmospheric circulation is assumed for time series beyond the instrumental era. This stationary assumption is questionable since proxies are stationary in time and space; however, this property does not apply to atmospheric patterns (Hernández et al., 2020). Another limitation of proxy reconstructions arises since proxy data is not a direct record of the atmospheric constitution. Instead, the interaction of the atmospheric mode with the biogeochemical and physical properties of the respective proxy is represented (Hernández et al., 2020). A single proxy, thus, represents the regional climatic state solely, while multi-proxy approaches diminish the uncertainty caused by this local teleconnection. In addition, climate models can be applied to refine the reconstructions of the atmospheric variability (Lee et al., 2019).

Despite the high amount of recent proxy-based reconstructions, the governing mechanisms behind the year-to-year and decadal-scale fluctuations of the atmospheric modes remain debated. Possible explanations of the observed variations are internal variability (e.g., non-linear interactions among atmospheric modes) or external forcings (e.g., solar effects or anthropogenic forcing) (Mann et al., 2020). Nonetheless, none of the proposed drivers sufficiently explain the observed variability and, thus, hinder the process of accurate predictions of regional climate effects (Hernández et al., 2020).

The *GreenPlanning* project provides an approach to increase the understanding of the atmospheric variability's mechanisms in the North Atlantic region. The concept proposes a relationship between the Greenland Ice sheet and the large-scale atmospheric circulation over the North Atlantic. Here, meltwater influx from the Greenland ice sheet into the Labrador Sea can decrease the deep-water formation. Subsequently, a cooling of the ocean region south-east of Greenland occurs, which is apparent in current observations. Future reduction of deep-water formation could cause the slowdown of the Gulf Stream (Rahmstorf et al., 2015) and, thus, influence the Atlantic storm

track. As a result, less humid and warm air could be transported to northern Europe, causing subarctic conditions in northwestern Europe (Dansgaard et al., 1993). However, this relationship is not robust, as other studies state that cooling of the subpolar gyre by freshwater leads to an enhancement of the North Atlantic storm track (Woollings et al., 2012). The research of this hypothesis incorporates the potential of substantial contribution to a more advanced understanding of the North Atlantic atmospheric variability. Furthermore, this contributes to an improvement of climate predictions, especially in the context of the expected future increase of the Greenland ice sheet's melting rates (IPCC, 2019).

3 Methodology

3.1 ERA5 Dataset

The analysis of this study is based on the *ERA5* dataset (Hersbach et al., 2018a; Hersbach et al., 2018b) for the period 1979-2021 and its back extension (*ERA5 BE*) (Bell et al., 2020a; Bell et al., 2020b) covering the years 1950-1978. *ERA5* is the fifth generation of an atmospheric reanalysis of the global climate produced by the *Copernicus Climate Change Service* (*C3S*) at the *European Centre of Medium-Range Weather Forecasts* (*ECMWF*). The dataset provides hourly estimates of different climate variables with a horizontal resolution of 31 kilometers and 137 vertical levels up to 80 kilometers. Moreover, daily and monthly aggregates of the hourly fields are available and "single level" data can be obtained, including 2D-parameters such as precipitation or vertical integrals over the entire depth of the atmosphere.
The dataset is produced using *Cy41r2* of the *ECMWF Integrated Forecast System* (*IFS*) which was applied for operational medium-range weather forecasting (Hersbach et al., 2020). This atmospheric model is coupled to a land-surface model (*HTESSEL*), producing e.g., the two-meter temperature, and an ocean wave model (*WAM*). The model data is combined with observations from across the world to a globally complete and consistent reanalysis product. The principle used to combine the model and observational data is called data assimilation. This method is used as well by numerical weather prediction centers. It combines a previous forecast in regular time intervals with an observation to generate an estimate of the state of the atmosphere, called analysis, which is then used to issue an improve forecast. In reanalysis this method is applied in reduced resolution to allow the dataset to span back several decades.
Moreover, a huge variety of observations is used e.g., satellite data, land station data, ship station data, aircraft data and radiosondes. The *ERA5 BE's* observational data relies on less advanced measurements with lower spatial and temporal resolution compared to the *ERA5* observational data. Nonetheless, the quality of this dataset is satisfactory for this analysis as severe limitations are apparent mainly in the accuracy of tropical cyclone intensity. In terms of the selected study area, this limitation can be neglected as solely subtropics to cold climate zones are of interest. The *ERA5* dataset and its back extension are accessible through the *C3S Climate Data Store* (*CDS*) in an interpolated format with regular latitude-longitude grid (Hersbach et al., 2020). The analysis conducted in this study uses monthly averaged data of mean sea level pressure [Pa] (*MSLP*), geopotential height at 500 hPa [m] (*GP500*), total precipitation [m] (*TP*), and two-meter temperature [K] (*TAS*). *GP500* is not directly accessible but has to be calculated by dividing the variable geopotential [m^2 s^{-2}] by the Earth's gravitational acceleration, g (9.80665 m s^{-2}).

3.2 Research Area and Period

All acquired data covers the North Atlantic region (20-85°N/80°W-40°E) for the period 1950-2021 as the signature of the *NAO* and other relevant modes of variability are strongly regional (Hurrell, 1995). The studied period is the maximal available time series of the *ERA5* dataset at the time of the analysis, representing a high-resolution record of the global atmosphere, land surface and ocean waves (Hersbach et al., 2020). Hence, a robust and concise analysis of the different atmospheric modes of variability and their relationship with the predictand variables temperature and precipitation is possible. The monthly-mean data of the respective variables for the whole study period have been obtained. Yet, the focus of this analysis relies on the extended winter season from November to March (NDJFM), as the climate variability in the winter season is mainly explained by the aforementioned modes of variability and a stronger effect local climate (Cortesi et al., 2021). However, results of single month and the different season have been analyzed and compared with each other prior to the main analysis.

3.3 Data Preprocessing

To evaluate the *ERA5* data, the software *CDO* (*Climate Data Operators*) (Schulzweida, 2021) and *python*[1] were used. The exemplary structure of a *CDO* command is as follows:

$$cdo\ command\ infile\ outfile. \tag{1}$$

The *ERA5* and *ERA5 BE* data on the *CDS* is filed in *grib* format and has been changed to *NetCDF* for further analysis. The two separate data files were merged together to a continuous file from 1950-2021. The analysis aims to analyze the climate variability independently of its trend, hence, the data was linearly detrended using:

$$X(t,s) = I(t,s) - (a(s) + b(s)\,t). \tag{2}$$

To acquire the detrended data matrix, $X(t,s)$, a least-square fit for every field element, s, over the time series, t, was calculated and the resulting function, $a(s)+b(s)\,t$, was subtracted from the initial data, $I(t,s)$. Subsequently, the monthly values of the whole year were split to create a dataset

[1] *python* code is available on *github* via https://github.com/SimonHesel/Master_Thesis_Simon_H/

covering merely the extended winter seasons. Furthermore, the mean value of each extended winter season was calculated, resulting in 71 values. The *five-year running mean* was calculated by computing the mean of each data point and the two preceding and two following seasons, resulting in 67 timesteps.

Furthermore, a particular interest of this study lies on more extreme anomalous winter conditions. Hence, the informative values of different sub-regions have been compared and a more precise analysis of the Northern Europe (45-75°N/10°W-40°E) has been conducted. The domain features the characteristic weather of northern Europe and stands in a contradictory relationship to the climate of southern Europe. As the weather conditions of over land are of particular interest, all ocean regions have been masked out. More extreme years were defined as the 25th and 75th percentile (first and third quartile) of the respective temperature and precipitation field mean for the whole study period, resulting in 18 timesteps. The analysis defining the coldest, warmest, driest, and wettest years of the domain are presented in the appendix (figure A.2).

3.4 Empirical Orthogonal Function Analysis

The preprocessed data has been analyzed by applying an *empirical orthogonal function analysis* (*EOF*) analysis. This method is widely used in meteorology and climate science to study the large-scale temporal and spatial variability of extensive datasets. It decomposes a meteorological space-time field into a set of orthogonal spatial patterns along with a set of associated *principal component time series* (*PCs*). The *EOFs* (eigenvectors) and *PCs* of the dataset represent a set of fixed spatial patterns and the respective loading of the pattern for every timestep. Furthermore, the amount of the variance, explained by the respective *EOFs* can be calculated. However, the method is purely mathematical and, thus, the interpretation of the results has to be done with caution. A major constraint is represented by the fact that physical modes are not necessarily orthogonal. Furthermore, it has to be noted that the sign of the respective *principal component* (*PC*) at a certain grid cell is interchangeable and not transferable to an information about the state of, e.g., a pressure center. The *EOF* analysis of this study has been done by using the *eofs pyhton library* provided by Dawson (2016), guaranteeing correctness and reproducibility of the results.

Prior to the analysis of spatial variability, the latitude-longitude grid has to be correctly weighted due to the convergence of the meridians. This has been done by calculating a weigthing factor ($wgts$),

$$wgts = \sqrt{cos(latitude)}. \tag{3}$$

Furthermore, the variation of the variables relative to the climatological normal (anomaly) has been computed by subtracting the mean field $\overline{X}$ for every timestep (t) and grid point (s),

$$A(t,s) = X(t,s) - \overline{X}(t,s). \tag{4}$$

The *EOFs* where calculated following the equation of Lorenz (1956),

$$A(t,s) = \sum_{k=1}^{M} P_k(t) \times E_k(s), \tag{5}$$

where M represents the number of analyzed *EOFs*, $\mathrm{E_k(s)}$ documents the *EOFs* (eigenvector) in space (s), and $\mathrm{P_k(t)}$ the *PCs* (t), presenting the amplitude of the respective *EOF*.

In general *EOF* analyses, the covariance matrix is then calculated and, subsequently, the eigenvalue problem solved. However, a computationally more efficient approach is to apply *single value decomposition* (*SVD*) (Golub and van Loan, 2013), as no covariance matrix has to be calculated. In the *SVD* approach, only singular values that are non-zero values are calculated as zero-values represent the mean field. The equation:

$$SVD(A) = U \Lambda V^T \tag{6}$$

describes that the SVD of the anomaly matrix, A, leads to the singular vectors in columns U and V, with the singular values in the leading diagonal of Λ. The singular vectors in column V are the *EOFs* and the singular values document a measure of the variance of the data, usually presented in percentage. The matrix is sorted in a decreasing order of the eigenvalues, hence, the eigenvector accounting for the highest share of the variance is the leading *EOF*. The respective *PCs* are computed by projecting the anomaly matrix, A, onto the *EOFs* and, subsequently, are scaled to unit variance.

The uncertainties of the respective eigenvalues have been computed by *North's rule of thumb* (North et al., 1982),

$$\begin{aligned} \Delta {\lambda_k}^2 &\sim \Delta {\lambda_k}^2 \sqrt{\frac{2}{n^*}} \\ \Delta \mathbf{u}_k &\sim \frac{\Delta {\lambda_k}^2}{{\lambda_j}^2 - {\lambda_k}^2} \mathbf{u}_j, \end{aligned} \tag{7}$$

to determine the number of analyzed *EOFs*. The spectra of the covariance matrices of extended winter seasonal *MSLP* and *GP500* (appendix figure A.1) demonstrate that the difference between the first *EOFs* and the subsequent ones is statistically independent, as the 95 % confidence interval (CI) error bars are not overlapping (Payton et al., 2003). The second to fourth eigenvalues and their 95 % CI error bars are relatively close and exhibit overlapping error bars, making demarcation difficult. However, the analysis covers the leading four *EOFs* as they explain over 80 % of the variability and since the inclusion of further *EOFs* would not lead to a substantial increase.

3.5 Principle Component Regression Analysis

In order to assess the relationship between the four leading *EOFs* and temperature and precipitation anomalies in the North Atlantic domain, a *PCR* analysis has been conducted. The method returns a linear regression coefficient by computing the least-square fit for each grid point in time. The results indicate information about the strength and direction of the relationship between the respective normalized *PC* and the anomaly field. Furthermore, Pearson's correlation coefficient (r) has been calculated,

$$r = \frac{cov(A, PC)}{\sigma_A \, \sigma_{PC}}, \tag{8}$$

expressing the correlation between each *PC* and the anomaly of the input dataset, A, at each grid point (see figures A.3, A.4, A.5, and A.6). The computed correlation coefficient is used to set a threshold of r=0.4 for the regression map to support the robustness of the archived results and its interpretability.

4 Results

4.1 EOF Analysis

4.1.1 Mean Sea Level Pressure and Geopotential Height at 500 hPa

Figure 4.1 shows the four leading *EOFs* of (a) *MSLP* and (b) *GP500* for the extended winter season covering the period 1950-2021. The total explained variance of all four leading *EOFs*, in the case of *MSLP*, is $\sim 6\,\%$ higher compared to *GP500*. Significantly, the first *EOF* (*EOF1*) of *MSLP* exceeds the explained variance of *GP500's* (*EOF1*) by $\sim 8\,\%$.

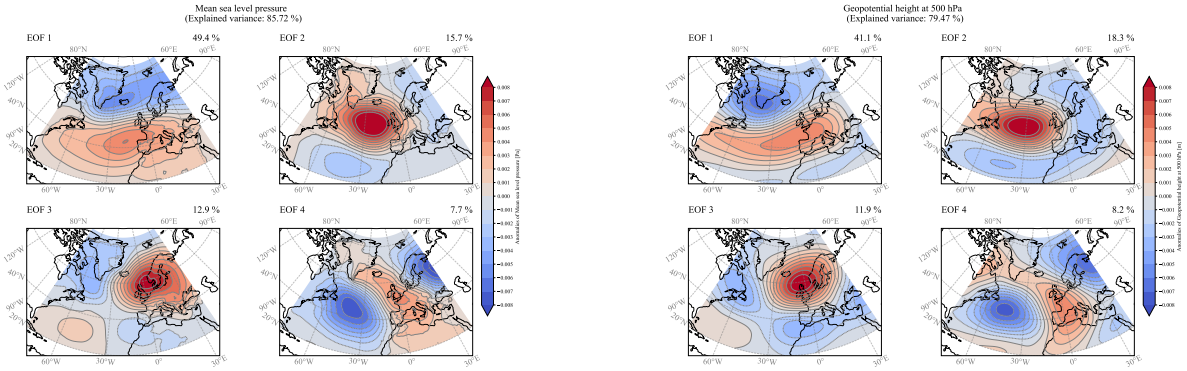

(a) (b)

Figure 4.1: The four leading *EOFs* of the extended winter seasonal (NDJFM) (a) *MSLP* and (b) *GP500* in the North Atlantic region calculated for the period 1950-2021. The explained variance of each individual *EOF* is displayed in the upper-right corner of every plot, and the total explained variance of the *EOFs* is shown on top of the four related maps.

The spatial patterns resemble each other; however, discrepancies are noticeable. The negative center of *EOF1* in the case of *GP500* is situated over the southern tip of Greenland, whereas *EOF1* of *MSLP* depicts a negative center that spans from southeast Greenland to north Fennoscandia. Furthermore, the positive center of *EOF1* of *GP500* is shifted slightly eastwards compared to the *EOF1* of *MSLP*. However, both *EOF1* resemble the spatial characteristics of the *NAO* mode, which is further on designated as the *NAO* pattern.
The second *EOF* (*EOF2*) patterns are remarkably alike, with a pronounced positive center over the North Atlantic Ridge. This pattern is henceforth called *East Atlantic* pattern. Yet, differences between the two divisions (a) *MSLP* and (b) *GP500* are apparent, as the center of the *MSLP* *EOF2* extends over parts of Greenland.
The third *EOF* (*EOF3*) features a quadruple pole situation in either case with a high magnitude

in northern Europe. However, a slightly stronger southeastern pole is noticeable for the *MSLP EOF3*. The described pattern is subsequently referred to as the *Northern European* pattern.
The fourth *EOF* (*EOF4*) illustrates a state with a positive center over western Europe and two negative centers, situated in northeastern Europe and, relatively centered, over the North Atlantic Ocean. Henceforward, similar patterns are referred to as *Western European* pattern. Comparing the *EOF4* in figure 4.1 demonstrates that the positive center of *MSLP* extends slightly more towards Greenland.
Further sections of the analysis focus on *MSLP* as it is widely used in preexisting studies, e.g., Hurrell (1995). In this regard, analyzing *MSLP* solely is sufficient to answer the research question since the *EOF* patterns (figure 4.1) present substantial consistency. Additionally, the explained variance of the leading four *EOFs* of *MSLP* is substantially higher than *GP500* and, hence, contains more information.

4.1.2 Mean Sea Level Pressure and Five-Year Running Mean

Figure 4.2 presents the results of the *EOF* analysis of (a) the extended winter seasonal mean and (b) its *five-year running mean* for the research period 1950-2021. The explained variance by the four leading *EOFs* is $\sim 3\,\%$ higher for the *five-year running mean*. Notably, *EOF1* accounts for $\sim 12\,\%$ more of the variability, while the other three *EOFs* explain less variability in comparison to the extended winter seasonal mean. *EOF1* and *EOF2* illustrate relatively consistent spatial patterns, yet, the action centers of the *five-year running mean* analysis feature a southward shift.

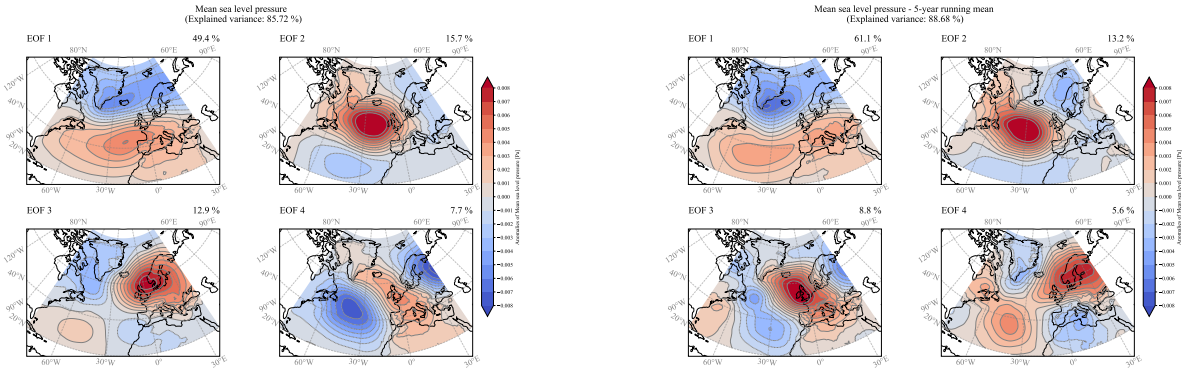

(a) (b)

Figure 4.2: The four leading *EOFs* of *MSLP* calculated for the (a) extended winter seasonal mean and (b) the *five-year running mean* of the extended winter season in the North Atlantic region for the period 1950-2021. The explained variance of each individual *EOF* is displayed in the upper-right corner of every plot, and the total explained variance of the *EOFs* is shown on top of the four related maps.

The *five-year running mean* analysis results present an exchange of the third and fourth *EOF*

patterns, as the *Northern European* pattern accounts for merely $\sim 6\,\%$ of the explained variance. In contrast, the explained variance of the *Western European* pattern increases slightly by $\sim 1\,\%$. Comparing the *Northern European* patterns, the action centers of the extended winter seasonal mean present a southward shifted positioning. The *Western European* pattern's main differences are the contrasting orders of magnitudes of the negative and positive centers.

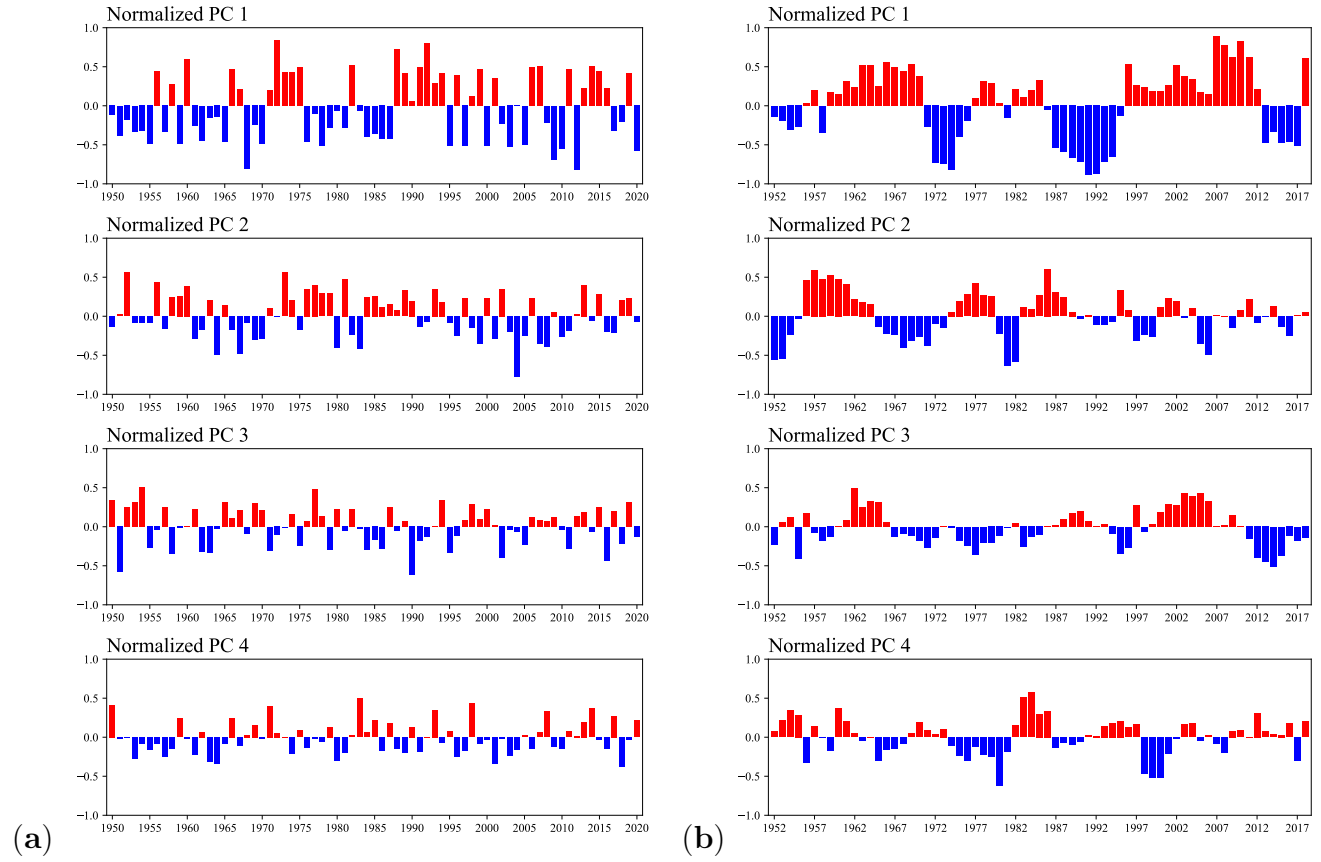

Figure 4.3: The normalized *PCs* of the respective *EOF* for the (a) extended winter seasonal mean and (b) the *five-year running mean* of the extended winter season in the North Atlantic region for the period 1950-2021. The number on the x-axis presents the year of (**a**) the respective November and December of the seasonal mean and (**b**) the respective November and December of the third year of the *five-year running mean*. Note that the x-axis of (**b**) covers 1952-2018. The spatial pattern of *PC3* in (**a**) corresponds to *PC4* in (**b**) and vice versa.

The normalized *PCs* (figure 4.3) presents the loading of the corresponding *EOF* in the respective extended winter season. All four *PCs* demonstrate a non-periodic oscillation, with the *EOF1* generally showing the highest loading. A smoothed course is apparent for the *PCs* of the *five-year running mean* with steadier positive or negative phases. Thus, the year-to-year variability is damped, increasing the influence of the *NAO* and *Western European* pattern. Repressing the annual variability causes an underrepresentation of anonymously high single-year events, e.g., *PC2* in the winter season 2004/05.

4.2 Principal Component Regression

4.2.1 Mean Sea Level Pressure and Total Precipitation

Figure 4.4 presents the *PCR* results of *MSLP* and total precipitation anomalies for the (a) extended winter seasonal mean and (b) the *five-year running mean* of the extended winter season in the North Atlantic region for the period 1950-2021. The regression of the *NAO* pattern and total precipitation anomalies features amplified positive coefficient values ranging from Greenland's southeast coast to the Norwegian west coast. Negative coefficient fields are located at the Atlantic coast of the Iberian Peninsula, expanding to the Azores, in southeastern Europe, and at the Italian Peninsula. A weaker negative regression is also apparent in northwest Greenland and along the Baffin Bay, while this relationship is spatially vaster for the *five-year running mean* analysis.

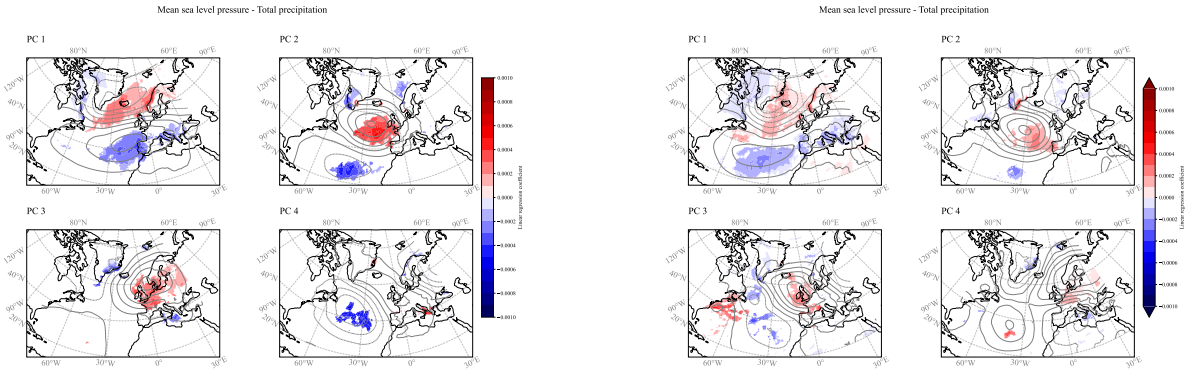

(a) (b)

Figure 4.4: *PCR* analysis of *MSLP* and total precipitation anomalies for the (a) extended winter seasonal mean and (b) the *five-year running mean* of the extended winter season in the North Atlantic region for the period 1950-2021. Grid boxes with a correlation coefficient (r) of less than 0.4 are white. Grey contour lines indicate the respective *EOF* pattern with negative values in dashed and positive in solid lines. Note the different color scales between the regression results of total precipitation and two-meter temperature (figure 4.5).

The *East Atlantic* pattern and precipitation anomalies present a pronounced positive regression spatially in accordance with the center of action over the North Atlantic Ocean and its adjacent coasts of the British Isles, France, and Spain. Furthermore, small-sized positive regression spots are located on the southeastern tip of Iceland and at a southeastern site in Greenland. Areas with negative regression coefficients are situated at the southwestern part of Greenland, presenting a divide with the positive regression field. Furthermore, a negative regression field is located in line with the action center at the southern part of the North Atlantic Ocean. An area with weak regression is in proximity to the northern Norwegian coast.

The regression between the *Northern European* pattern and total precipitation anomalies reveals an

enhanced positive relationship in northwestern Europe and at the southeastern coast of Greenland, South Iceland, Svalbard, and south of the Italian Peninsula. The *five-year running mean* results generally reveal weaker regression; however, the overall patterns are similar.
The *Western European* pattern of the extended winter seasonal mean presents positive regressions coefficients for small spots at the central-eastern coast of Greenland, the southern part of the Adriatic Sea, and the northern coast of the Iberian Peninsula. Negative regression coefficients are apparent in accordance with the action center at the North Atlantic Ocean and with less magnitude scattered along the Norwegian coast. The regression results of the *five-year running mean* (figure 4.4, (b), *PC3*) present a higher number of positive and negative regression fields. The positive regression areas are situated over the British Isles, western Europe, the eastern coast of Iceland, and along the east coast of North America. One further negative regression area is located at the southern tip of Greenland.

4.2.2 Mean Sea Level Pressure and Two-Meter Temperature

The results presented in Figure 4.5 are the *PCR* of *MSLP* and two-meter temperature anomalies for the (a) extended winter seasonal mean and (b) the *five-year running mean* of the extended winter season in the North Atlantic region for the period 1950-2021.
The *NAO* pattern demonstrates positive regression fields in northern Europe and the southeast coast of North America. Negative regression coefficients are illustrated at northeastern America and large parts of Greenland, with the exception of the north and east Greenlandic coast. Further negative regression values are depicted at the southern and eastern parts of the Mediterranean. The *five-year running mean* results generally feature a weaker regression signal.
The *East Atlantic* pattern and the two-meter temperature present, in the case of the extended winter seasonal mean, positive regression hotspots at the southwestern part of the Mediterranean and the southwestern region of the North Atlantic. In contrast, the *five-year running mean* mean illustrates a positive regression field, particularly at central Greenland and its southeastern coast. Negative regression fields are situated in accord with the action center at the North Atlantic Ocean and extend towards its adjacent North American coast. In contrast, the *five-year running mean* results of the *East Atlantic* pattern do not present negative regression areas above the 0.4 correlation coefficient threshold (figure 4.5, (b), *PC2*).
Regression results for the *Northern European* pattern reveal fields with positive regression coefficients at southeastern Europe and Anatolia. Negative regression areas are situated along the east coast of Greenland and in Iceland. The *five-year running mean* regression features a locally positive coefficient field north of the Black Sea.
The *Western European* pattern presents a positive regression field close to the east coast of the

North American continent. In the case of the *five-year running mean* , another positive regression spot is located in southeastern Europe. Negative regression areas of the extended winter seasonal mean are solely small spots along the north-western African coast. In contrast, the *five-year running mean* regression presents negative regression fields only at the North Atlantic region south of Greenland and Iceland.

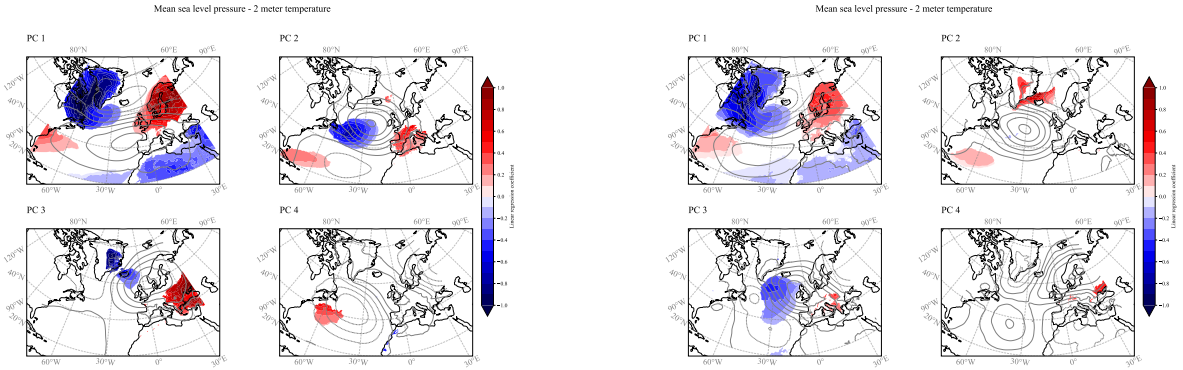

(a) (b)

Figure 4.5: *PCR* analysis of *MSLP* and two-meter temperature anomalies for the (a) extended winter seasonal mean and (b) the *five-year running mean* of the extended winter season in the North Atlantic region for the period 1950-2021. Grid boxes with a correlation coefficient (r) of less than 0.4 are white. Grey contour lines indicate the respective *EOF* pattern with negative values in dashed and positive in solid lines. Note the different color scales between the regression results of total precipitation (figure 4.4) and two-meter temperature.

4.3 Precipitation and Temperature Quartiles of the Northern European Domain

4.3.1 EOF Analysis

The four leading *EOFs* of the dry quartile present the relatively highest explained with $\sim 89\,\%$, whereas the *EOF* analysis of the warm quartile accounts for merely $\sim 82\,\%$ of the total variance (figure 4.6).

Comparing the spatial structure of the first *EOF*, the (a) cold, (c) dry, and (d) wet quartiles display similarities resembling the *NAO* pattern. Yet, the (a) cold and (c) dry quartiles present a pronounced center at the southern tip of Greenland, whereas the *EOF1* of the (b) wet quartile depicts a center over the Norwegian Sea with a wider expansion. Moreover, the positive center of the (d) wet quartile is shifted northwards, presenting a centered pattern over the North Atlantic Ocean. The explained variance by *EOF1* of the dry and wet quartile documents a difference of

$\sim 3\,\%$, whereas the difference between the dry and cold quartile is $\sim 13\,\%$. Although the *EOF* analysis of the warm quartile does not represent a clear *NAO* pattern in one of the *EOFs*, the third *EOF* structure depicts structural similarities.

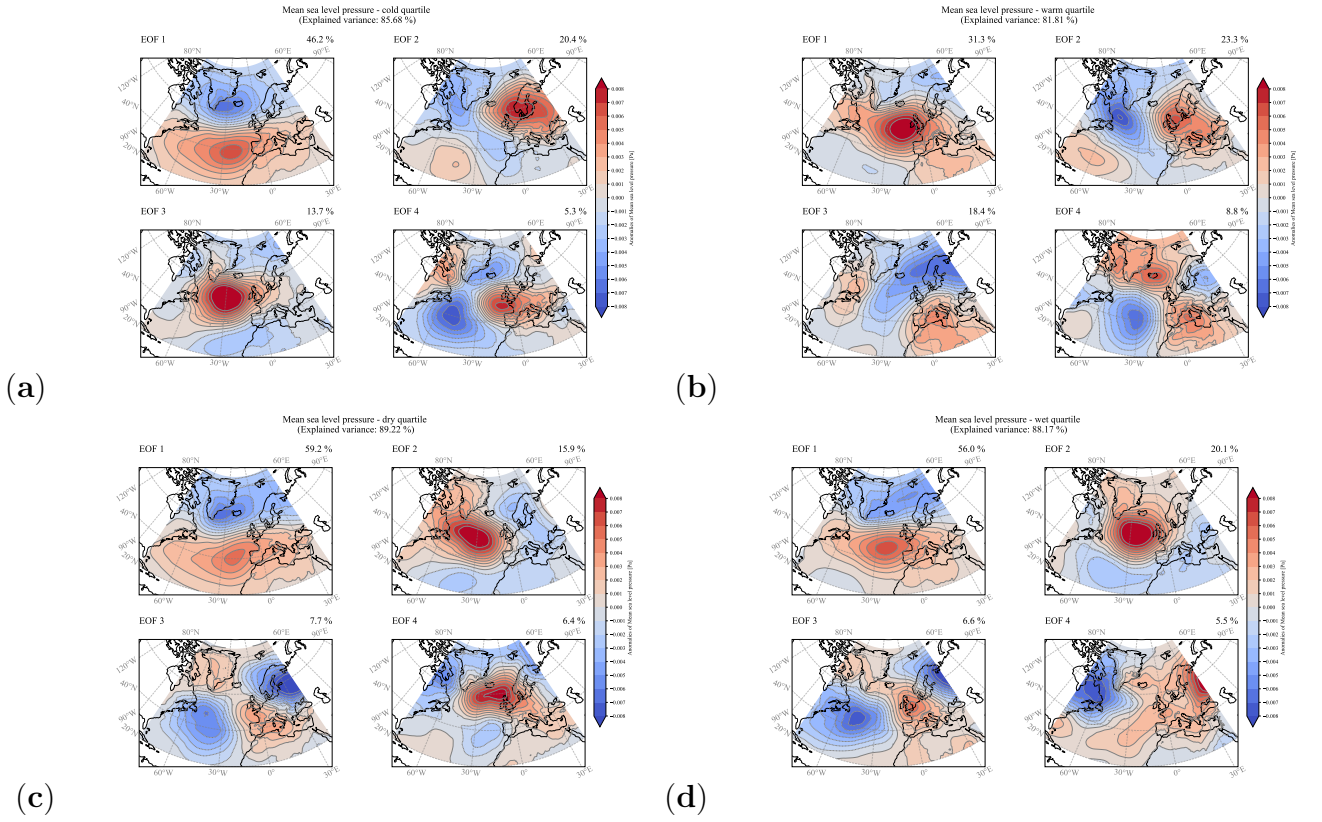

Figure 4.6: The four leading *EOFs* of *MSLP* in the North Atlantic region calculated for the (a) cold, (b) warm, (c) dry, and (d) wet quartiles of the Northern European domain over the period 1950-2021. The explained variance of each individual *EOF* is displayed in the upper-right corner of every plot, and the total explained variance of the *EOFs* is shown on top of the four related maps.

The first *EOF* of the (b) warm quartile accounts for $\sim 31\,\%$ of the variance and depicts a pronounced center over the North-Atlantic, resembling the *East Atlantic* pattern. The other quartiles present similar spatial structures in *EOF3* of the (a) cold quartile, *EOF2* of the (c) dry quartile, and *EOF2* of the (d) wet quartile; however, the expansion patterns differ.

The *Northern European* pattern is resembled by *EOF2* of the (a) cold and (b) warm quartile, and by the *EOF4* of the (c) dry and (d) wet quartile. This pattern is characterized by a pronounced positive action centers over Fennoscandia and the southwestern part of the North Atlantic Ocean, and a negative area located at eastern North America and Greenland. Differences in this structure are apparent analyzing *EOF2* of the (b) warm quartile, where a southward shift of the northern action centers is visible. The *EOF4* of the (c) dry quartile presents a westward shifted positive cen-

ter located at Iceland and the British Isles. Furthermore, *EOF4* of the (d) wet quartile documents spatial discrepancies, as the positive action center is shifted eastward and spatially expanded over large parts of the domain. The negative center instead is shifted westwards and pronounced. The explained variance by *EOF2* of (a) the cold-quartile is $\sim 20\,\%$ and, thus, similar to *EOF2* of the (b) warm-quartile. In contrast, the *Northern European* patterns of the (c) dry and (d) wet quartile account for approximately $6\,\%$ of the variance.
The spatial structures presented by *EOF4* of the (a) cold and (b) warm quartile, and by *EOF3* of the (c) dry and (d) wet quartile resemble the West Atlantic pattern. Calculations of the explained variance by this pattern range from 5 to $9\,\%$. The spatial distribution varies with the (a) cold quartile presenting a westward shift of the northern center, spatially expanding over Greenland, and with the (b) warm quartile, mapping a more pronounced positive northern center, located over Iceland. Both patterns illustrate a noticeable quadrupole state.

4.3.2 Principal Component Regression

4.3.2.1 Mean Sea Level Pressure and Total Precipitation

The *NAO* pattern is resembled by *EOF1* of the (a) cold, (c) dry, and (d) wet quartile and *EOF3* of the (b) warm quartile. Positive *PCR* results with total precipitation anomalies are particularly apparent between the Greenlandic east coast and the western coast of Norway. The (b) warm quartile, though, presents opposite singed regression coefficients for the east coast of Greenland and a less pronounced positive signal in the Norwegian area. In contrast, a positive regression field is located in the Baltic region, which is also apparent in the (a) cold quartile. Another deviating feature is represented by the *PCR* of the (d) wet quartile, where a positive regression spot is located at the southern tip of Greenland. Similar to the results of the whole study period, negative regression fields of the *NAO* pattern and total precipitation anomalies are located in Southern Europe and the North Atlantic Ocean, expanding from the European coast to the Azores. Irregularities occur again for *EOF3* of the (b) warm quartile, where the negative regression field represents only a minor expansion in the central Mediterranean region.
The *East Atlantic* pattern is present in *EOF3* of the (a) cold quartile, in *EOF1* of the (b) warm quartile, and *EOF2* of the (c) dry and (d) wet quartile. Comparing the corresponding regression coefficient maps documents similarities between all quartiles, such as a dipole between a positive and negative regression field at southern Greenland. Furthermore, a positive regression area is situated in accordance with the *EOF* pattern at the North Atlantic ridge. Differences mainly concern the expansion of the aforementioned regression area and the occurrence of a positive regression field at the North American coast, apparent in the (c) dry and (d) wet quartile. The distribution of

the negative regression areas presents stronger deviations between the different quartiles. One field is situated at the Atlantic coast of Norway, though the (d) wet quartile does not present regression coefficients with a correlation above the 0.4 threshold for that area. Further negative regression values are apparent west of the African continent and at the central-eastern Mediterranean region.

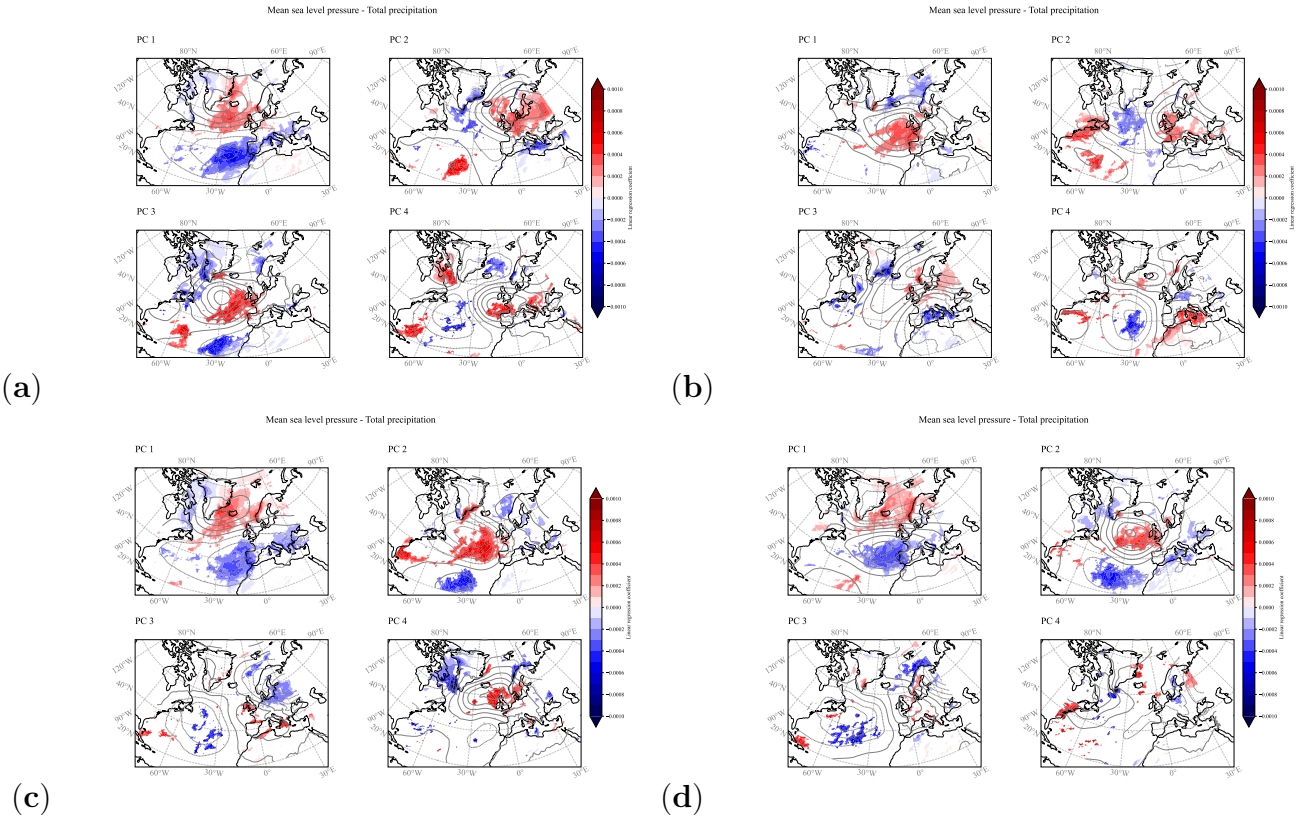

Figure 4.7: *PCR* analysis of *MSLP* and total precipitation anomalies in the North Atlantic region calculated for the (a) cold, (b) warm, (c) dry, and (d) wet quartiles of the Northern European domain over the period 1950-2021. Grid boxes with a correlation coefficient (r) of less than 0.4 are white. Grey contour lines indicate the respective *EOF* pattern with negative values in dashed and positive in solid lines. Note the different color scales between the regression results of total precipitation and two-meter temperature (figure 4.8)

The *Northern European* pattern is present in *EOF2* of the (a) cold and (b) warm quartile, and in *EOF4* of the (c) dry and (d) wet quartile. Comparing the four quartiles reveals many deviations, especially in the case of the (c) dry and (d) wet quartile. However, positive regression areas can be found in central and northern Europe, particularly present in the (a) cold quartile. Notable, the Scandic Mountain range divides the positive from a negative regression field, apparent in the (c) dry quartile. The (b) warm and (d) wet quartile, furthermore, document a positive regression area along the North American Atlantic coast. Specific positive regression spots are located along the Greenlandic eastern coast in the case of the (c) dry and (d) wet quartile. A negative regres-

sion area is located at the southern coast of Greenland, though different expansion patterns are apparent. Especially, the (c) dry quartile presents a vaster prolongation towards the Greenlandic West coast and the North American continent. Further negative regression spots are located at the Mediterranean (figure 4.7, (a) (c)) and at the northern Norwegian coast (figure 4.7, (b) (c)). The spatial structures presented by *EOF4* of the (a) cold and (b) warm quartile, and by *EOF3* of the (c) dry and (d) wet quartile resemble the West Atlantic pattern. The regression patterns of the quartiles deviate substantially. Positive regression fields are in proximity to the southeastern coast of the North American continent. The (a) cold and (c) dry quartiles present positive regression areas at the west European coast and southeastern Europe, where the (b) warm and (d) wet quartiles also localize respective fields. An inconsistent regression field is located at the Labrador Sea occurring on the *PC4* plot of the (a) cold quartile. Additionally, the (c) dry and (d) wet quartiles present positive regression spots at the Greenlandic southeast coast. Negative regression areas are found in accordance with the action center at the North Atlantic Ocean. Locations on land deviate a lot. The Norwegian coast presents negative regression values in the case of the (a) cold and (c) dry quartile; however, the (b) warm quartile documents a positive field here. Another area with negative regression values is situated in the Baltic area (figure 4.7, (b), (c)).

4.3.2.2 Mean Sea Level Pressure and Two-Meter Temperature

The *NAO* pattern and two-meter temperature anomalies present positive regression areas in central to northern Europe and at the southeastern North American coast, although the European field is most pronounced in the (c) dry quartile. Profound deviations are apparent for the (a) cold quartile, where the European signal is damped and, instead, a positive regression area is represented along the eastern Greenlandic coast. Furthermore, the (b) warm quartile rather documents a positive regression field along the European and North African coast, while the North American spot is shifted northwards. Distinct negative regression areas are located at between Greenland and North America and at northern Africa and the eastern Mediterranean region. However, discrepancies are apparent for the (c) warm quartile, localizing negative regression spots solely in Greenland and northeastern Africa.
The *PCR* analysis of the *East Atlantic* pattern and the two-meter temperature reveal a common positive regression field at southwestern Europe apparent in the (a) cold, (c) dry, and (d) wet quartile, while the wet quartile reflects a spatial expansion to northern Europe. The (b) warm quartile also presents a European regression field, though its spatial distribution is localized in central to southern Europe and, further, North Africa. Another positive regression area is located at Greenland and northern America, especially noticeable at the (b) warm quartile. Negative coefficient values are less distributed, although a respective regression field is in proximity to the

eastern North American coast. Furthermore, the (a) cold and (b) warm quartile also feature a negative regression spot on the Scandinavian Peninsula.

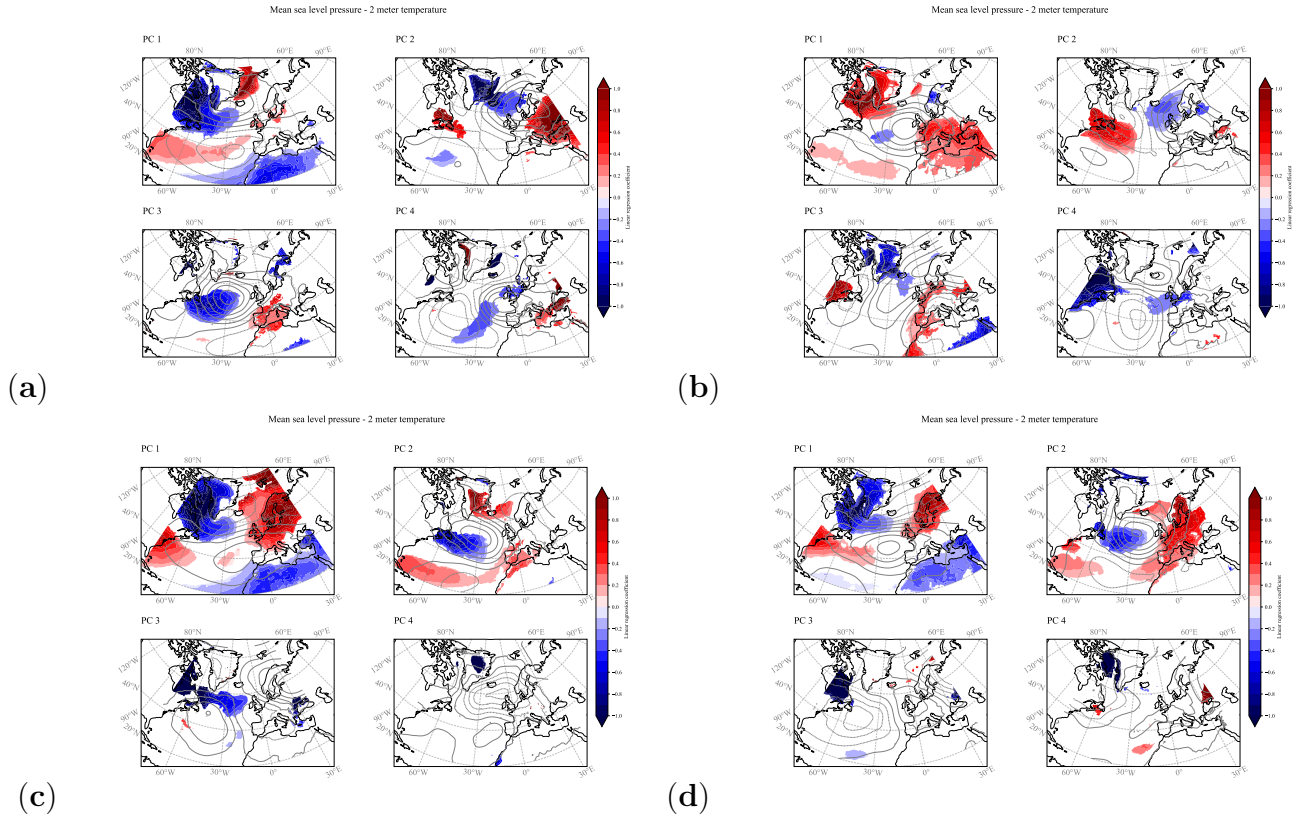

Figure 4.8: *PCR* analysis of *MSLP* and two-meter temperature anomalies in the North Atlantic region calculated for the (a) cold, (b) warm, (c) dry, and (d) wet quartiles of the Northern European domain over the period 1950-2021. Grid boxes with a correlation coefficient (r) of less than 0.4 are white. Grey contour lines indicate the respective *EOF* pattern with negative values in dashed and positive in solid lines. Note the different color scales between the regression results of total precipitation (figure 4.7) and two-meter temperature

The *Northern European* pattern maps positive regression areas with the two-meter temperature at the East coast of North America, particularly Newfoundland, with strong signals for the (a) cold and (b) warm-quartile. Moreover, a positive regression field is located at eastern Europa and Anatolia, represented in the (a) cold, (b) warm, and (d) wet quartile. Notably, the (c) dry and (d) wet quartile represents only minor regression areas for the *Northern European* pattern. However, common negative regression fields are situated on Greenland, with the (d) wet quartile also covering the Baffin Bay. The (b) warm quartile does not present negative regression spots on Greenland and, instead, illustrates a field around Iceland and the Baltic area.
Positive regression areas of the regression with the West Atlantic pattern and the two-meter temperature are located at the eastern Mediterranean and at the northwestern Greenlandic coast

(figure 4.8, (a), *PC4*). The other quartiles merely present scattered positive regression spots. On the other hand, a pronounced negative regression field is apparent in the (b) warm, (c) dry, and (d) wet quartiles located at the northwestern coast of North America. The (a) cold and (b) warm quartiles, furthermore, feature a negative regression area at northwestern Europe.

5 Discussion

5.1 EOF Analysis

The results of the *EOF* analysis demonstrate substantial deviations between the respective total explained variance. Smoothening the *MSLP* extended winter seasonal mean dataset by calculating the *five-year running mean* increases the significance of the first mode of variability. Hence, the *NAO* pattern seems to be the governing mode of decadal variability.
In contrast, the *East Atlantic* pattern and, particularly, the *Northern European* pattern significantly lose influence on longer timescales. This loss of influence impedes the feasibility of reconstructing the variability modes as far-reaching proxy records usually present a coarser temporal resolution.
The high total explained variance values of the dry and wet quartile demonstrate the strong relationship between the atmospheric modes of variability and precipitation anomalies in the Northern European domain. Again, the *NAO* pattern reveals to be the dictating mode of variability, constituting an exceptionally high share of the explained variance. Contradicting results are apparent for the temperature quartiles, indicating a weaker importance of the *NAO* on the Northern European temperature anomalies. In contrast, the *Northern European* and *East Atlantic* patterns seem to play a more significant role. The warm quartile represents a comparably low explained variance by the four leading *EOFs*, concluding a decreased significance of the defined modes of variability. This finding resembles previous analyses of the Northern Atlantic atmospheric variability of the summer month, where the mean sea level pressure presents a much more uniform equator-to-pole distribution (Hurrell et al., 2003).
The diverging spatial distribution of the defined *EOF* patterns results from the discrepancies between the *MSLP* fields of the analyzed years. A substantial deviation of the characteristic *NAO* pattern is apparent in the warm quartile, concluding that years with positive temperature anomalies in Northern Europe are not accompanied by the typical *NAO* pattern. This asymmetry is an important finding, questioning the relevance of the *NAO* pattern in a world with more warmer winters.
The eastward shifted *NAO* pattern, apparent in the wet and warm quartile, corresponds to a positive *NAO* state. Similarly, a negative *NAO* state, represented in the dry and cold quartile, is characterized by a pronounced center of action at the southern tip of Greenland. Both findings are supported by Hurrell *et al.* (2003) and align with the characteristic weather states in the Northern European domain defined by the respective *NAO* state. Expected wetting and warming of the Northern European winter climate contribute to the assumption that future climate might be accompanied by a higher amplitude of positive *NAO* states. For that matter, these results align

with the findings of Lu and Greatbatch (2002), documenting an eastward shift of the predominant *NAO* pattern in the last 40 years of the 20th century, where a significant climate warming was apparent.
The temperature and precipitation quartile *EOFs*, resembling the *Northern European* pattern, present substantial deviations of the explained variance. Hence, it can be assumed that similar *MSLP* patterns of the precipitation quartiles are underrepresented compared to the temperature quartiles. Nevertheless, the results do not elucidate the general occurrence of this pattern and its impact on the climate system, as it solely informs about its frequency.
The fact that the *Western European* pattern generally accounts for less than 10 % of the variance limits the importance and robustness of the respective *EOFs* as discussed by Dommenget and Latif (2002).

5.2 Teleconnection Patterns

The *PCR* results are discussed regarding reconstruction approaches, especially as a contribution to the *GreenPlanning project*.
Unique characterization of the *NAO* pattern is possible by analyzing precipitation anomalies at the southwestern coast of the Norwegian Peninsula and the central Mediterranean region. A positive (negative) precipitation anomaly at the northern (southern) area indicates an enhanced *NAO* state. In contrast, a negative *NAO* phase would cause a contradictory weather state. To produce a robust reconstruction of the *NAO* pattern, temperature anomalies could be analyzed for Denmark and north of the Red Sea, as these locations are consistently represented in all analyzed datasets. The findings align with the literature, supporting a strong relationship between the *NAO* and respective weather anomalies in the aforementioned fields (Hurrell and Van Loon, 1997). However, an even vaster relationship is pointed out in this analysis, which is mainly limited by the deviating *NAO* pattern of the warm quartile. Nonetheless, the fact that the here suggested regions represent a more robust relationship indicates a higher certainty of reconstruction approaches and further increases the understanding of the analyzed relationship, especially regarding temperature anomalous winter years of the Northern European domain. The quadrupole teleconnection pattern pointed out by Smith *et al.* (2020), with a positive correlation in northern Europe and southeast North America and a negative correlation in southern Europe and northeast North America, is represented in the results of all quartiles analyses. However, the warm quartile presents a northward shift in the western part and a southward shift in the eastern part of the domain. Hence, solely considering a quadrupole pattern does not sufficiently reflect the teleconnections as the exact locations of the relationship are crucial for robust reconstructions.
The *East Atlantic* pattern presents characteristic precipitation and temperature relationships. Sig-

nificantly, the precipitation seesaw in southern Greenland depicts a unique pattern that poses a useful coherency for reconstruction approaches. The interrelation can be explained as a pronounced high-pressure system at the East Atlantic location would increase the transport of wet air masses towards the Greenlandic southeast coast. Besides, a significant correlation between the *East Atlantic* pattern and temperature anomalies is located in the eastern part of the Iberian Peninsula and Newfoundland. However, the latter teleconnection is not apparent for the dry quartile. Still, the unique combination of the different interdependencies supports reconstruction approaches of the *East Atlantic* pattern. In conclusion, a positive (negative) *East Atlantic* state is related to higher (lower) than average temperatures in the Iberian Peninsula and precipitation in southeastern Greenland. Additionally, lower (higher) than average temperatures in Newfoundland and precipitation in southwestern Greenland would appear.

The *Northern European* pattern presents a unique precipitation teleconnection at the North Sea and eastern Greenlandic coast, though the latter relationship is not apparent in the dry quartile. A positive (negative) *Northern European* pattern corresponds to higher (lower) than normal precipitation values at the North Sea and a lower (higher) than normal values in east Greenland. Supported by the temperature relationship, mainly located north of the Black Sea and at the east Greenlandic coast, a unique *Northern European* teleconnection pattern has been identified. However, the precipitation quartiles of the Northern European domain do not show consistent relationships. This discrepancy can be explained by the spatial deviation from the defined *Northern European* pattern and the low explained variance. Taking this conclusion into account for reconstruction approaches poses a way to increase their accuracy.

Lastly, the *Western European* pattern can be identified by characteristic teleconnections at the Adriatic Sea and the Azores. A positive (negative) *Western European* state is associated with higher (lower) than normal winter precipitation values in the Adriatic sea region and lower (higher) than usual precipitation on the Azores. Temperature teleconnections are less uniform and, hence, present a vague indicator for the *Western European* pattern. The results enhance knowledge on the consistency of the atmospheric variability of the North Atlantic region and, subsequently, support reconstruction approaches, for instance, concerning the GreenPlanning project. Consequently, this study supports the overall understanding of the climate system of the Northern Atlantic region. Subsequently, it contributes to an increased climate predictability in this region, which is especially crucial regarding the experienced warming climate.

5.3 Limitations and Future Research

The conducted analysis depends on the chosen methods, hence, poses some limitations. Referring to this, *EOF* analysis struggles to provide a complete picture of the atmospheric features.

Especially, the *EOFs* with a lower explained variance seem to be degenerated and, thus, yield difficulties in interpretation. Future research could include comparing different statistical tools, such as regressions, VARIMAX, or rotated, extended, and complex *EOF* analysis (Hannachi et al., 2007). Consistency between all data representations allows more robust transfer to potential physical modes.

Furthermore, the defined correlation coefficient threshold of 0.4 might filter out locations that present a sufficient relationship in terms of reconstructing the atmospheric variability. Although the selection is arbitrary, it guarantees the robustness of the found regression results. However, this constraint could be overcome by applying other significant tests or comparing maps with other correlation coefficient thresholds.

The more extreme anomalous winter conditions of the defined Northern European domain provide insightful results. Certainly, a strong dependency on the prevailing climate conditions leads to a high uncertainty when transferring the findings to other regions. Future research could analyze different domains and compare the consistency of the results.

Although ERA5 presents a modern and sophisticated reanalysis dataset, deviations from the 'real world' are unavoidable (Hersbach et al., 2020). Further studies could compare the results with other observational data to verify the results. Moreover, a comparison with climate simulations would contribute to a better understanding and further increase the preciseness and validity of the reconstruction approaches, as mentioned in chapter 2.2.

A more sophisticated understanding of the observation relationships calls for the analysis of other climatic variables, e.g., surface pressure, ocean properties or storminess, as these parameters heavily influence the North Atlantic climate system and its influence on the weather in the region.

In terms of reconstruction of the atmospheric variability, the applicability of the findings is limited due to the temporal approach of this study. Proxy data containing information about the extended winter period is limited as it does not cover the growing season. Moreover, the study found a signal weakening when coarsening the temporal resolution. This process might imply significant constraints for reconstruction approaches.

6 Conclusion

In this study, I conducted an empirical orthogonal function analysis of mean sea level pressure in the North Atlantic region for the period 1950-2021. In doing so, I used the ERA5 reanalysis dataset to analyze atmospheric modes of variability during the extended winter season (NDJFM). Additionally, I performed a principal component regression analysis to examine the importance of the different climatic modes on weather conditions, with a particular focus on more extreme anomalous winter conditions.

The present findings confirm a strong influence of the climatic modes on the weather conditions in the North Atlantic domain. Particularly, the *NAO* demonstrates a governing role in the Northern Atlantic climate system. However, the study documents an unexpected asymmetry of the *NAO* pattern with respect to the temperature segregated analyses. This provides some crucial knowledge improvement in terms of reconstruction approaches and the general understanding of the atmospheric variability in the North Atlantic region.

Besides, this study demonstrates characteristic teleconnection patterns of the four leading variability modes. This may be considered a promising aspect of reconstruction approaches, particularly in the scope of the GreenPlanning project. Furthermore, the analysis contributes to a better understanding of the North Atlantic climate system and, hence, might help to increase the predictability of future climate. However, future investigations are necessary to validate the conclusions that can be drawn from this study. Corresponding recommendations include analyzing additional observational and climate model data, comparing with different methodological approaches, and examining other temporal resolutions and periods.

References

Athanasiadis, P. J., Yeager, S., Kwon, Y.-O., Bellucci, A., Smith, D. W., & Tibaldi, S. (2020). Decadal predictability of North Atlantic blocking and the NAO. *npj Climate and Atmospheric Science*, *3*(1), 20. https://doi.org/10.1038/s41612-020-0120-6

Becker, L. W. M., Sejrup, H. P., Hjelstuen, B. O., Haflidason, H., Kjennbakken, H., & Werner, J. P. (2020). Palaeo-productivity record from Norwegian Sea enables North Atlantic Oscillation (NAO) reconstruction for the last 8000 years. *npj Climate and Atmospheric Science*, *3*(1), 42. https://doi.org/10.1038/s41612-020-00147-6

Bell, B., Hersbach, H., Berrisford, P., Dahlgren, p., Horányi, A., Muñoz Sabater, J., Nicolas, J., Peubey, C., Radu, R., Schepers, D., Simmons, A., Soci, C., & Thépaut, J.-N. (2020a). ERA5 monthly averaged data on pressure levels from 1950 to 1978 (preliminary version). *Copernicus Climate Change Service (C3S) Climate Data Store (CDS). (Accessed on 01-02-2022)*. https://cds.climate.copernicus-climate.eu/cdsapp#!/dataset/reanalysis-era5-pressure-levels-monthly-means-preliminary-back-extension?tab=overview

Bell, B., Hersbach, H., Berrisford, P., Dahlgren, p., Horányi, A., Muñoz Sabater, J., Nicolas, J., Peubey, C., Radu, R., Schepers, D., Simmons, A., Soci, C., & Thépaut, J.-N. (2020b). ERA5 monthly averaged data on single levels from 1950 to 1978 (preliminary version). *Copernicus Climate Change Service (C3S) Climate Data Store (CDS). (Accessed on 01-02-2022)*. https://cds.climate.copernicus-climate.eu/cdsapp#!/dataset/reanalysis-era5-single-levels-monthly-means-preliminary-back-extension?tab=overview

Beniston, M. (2004). The 2003 heat wave in Europe: A shape of things to come? An analysis based on Swiss climatological data and model simulations. *Geophysical Research Letters*, *31*(2). https://doi.org/10.1029/2003GL018857

Bradley, R. S. (2015). Chapter 1 - paleoclimatic reconstruction. In R. S. Bradley (Ed.), *Paleoclimatology (third edition)* (Third Edition, pp. 1–11). Academic Press. 10.1016/B978-0-12-386913-5.00001-6

Christensen, J. H., Krishna Kumar, K., Aldrian, E., An, S.-I., Cavalcanti, I., de Castro, M., Dong, Q., Goswami, P., Hall, A., Kanyanga, J., Kitoh, A., Kossin, J., Lau, N.-C., Renwick, J., Stephenson, D., Xie, S.-P., & Zhou, T. (2013). Climate Phenomena and their Relevance for Future Regional Climate Change. *Climate Change 2013: The Physical Science Basis. Contribution of Working Group I to the Fifth Assessment Report of the Intergovernmental Panel on Climate Change* (pp. 1217–1308). Cambridge University Press. https://doi.org/10.1017/CBO9781107415324.028

Cortesi, N., Torralba, V., Lledó, L., Manrique-Suñén, A., Gonzalez-Reviriego, N., Soret, A., & Doblas-Reyes, F. J. (2021). Yearly evolution of Euro-Atlantic weather regimes and of their

sub-seasonal predictability. *Climate Dynamics*, *56*(11), 3933–3964. https://doi.org/10.1007/s00382-021-05679-y

Dansgaard, W., Johnsen, S. J., Clausen, H. B., Dahl-Jensen, D., Gundestrup, N. S., Hammer, C. U., Hvidberg, C. S., Steffensen, J. P., Sveinbjörnsdottir, A. E., Jouzel, J., & Bond, G. (1993). Evidence for general instability of past climate from a 250-kyr ice-core record. *Nature*, *364*(6434), 218–220. https://doi.org/10.1038/364218a0

Davini, P., Cagnazzo, C., Neale, R., & Tribbia, J. (2012). Coupling between Greenland blocking and the North Atlantic Oscillation pattern. *Geophysical Research Letters*, *39*(14). https://doi.org/10.1029/2012GL052315

Dawson, A. (2016). Eofs: A Library for EOF Analysis of Meteorological, Oceanographic, and Climate Data. *Journal of Open Research Software*, *4*(1). https://doi.org/10.5334/jors.122

Dommenget, D., & Latif, M. (2002). A cautionary note on the interpretation of EOFs. *Journal of Climate*, *15*(2), 216–225. https://doi.org/10.1175/1520-0442(2002)015⟨0216:ACNOTI⟩2.0.CO;2

Drouard, M., Kornhuber, K., & Woollings, T. (2019). Disentangling Dynamic Contributions to Summer 2018 Anomalous Weather Over Europe. *Geophysical Research Letters*, *46*(21), 12537–12546. https://doi.org/10.1029/2019GL084601

Edenhofer, O., Pichs-Madruga, R., Sokona, Y., Kadner, S., Minx, J., Agrawala, S., Baiocchi, G., Bashmakov, I., Blanco, G., Broome, J., Bruckner, T., Bustamante, M., Clarke, L., Conte Grand, M., Creutzig, F., Cruz-Núñez, X., Dhakal, S., Dubash, N., Eickemeier, P., & Zwickel, T. (2014). *Climate change 2014: Mitigation of climate change ; Working Group III contribution to the Fifth Assessment Report of the Intergovernmental Panel on Climate Change*. Cambridge Univ. Press. https://doi.org/10.1017/CBO9781107415416

Golub, G. H., & van Loan, C. F. (2013). *Matrix Computations* (Fourth). JHU Press. http://www.cs.cornell.edu/cv/GVL4/golubandvanloan.htm

Goosse, H. (2015). *Climate System Dynamics and Modelling*. Cambridge University Press. https://doi.org/10.1017/CBO9781316018682

Häkkinen, S., & Rhines, P. B. (2004). Decline of Subpolar North Atlantic Circulation During the 1990s. *Science*, *304*(5670), 555–559. https://doi.org/10.1126/science.1094917

Hannachi, A., Jolliffe, I. T., & Stephenson, D. B. (2007). Empirical orthogonal functions and related techniques in atmospheric science: A review. *International Journal of Climatology*, *27*(9), 1119–1152. https://doi.org/10.1002/joc.1499

Haylock, M. R., & Goodess, C. M. (2004). Interannual variability of European extreme winter rainfall and links with mean large-scale circulation. *International Journal of Climatology*, *24*(6), 759–776. https://doi.org/10.1002/joc.1033

Hernández, A., Martin-Puertas, C., Moffa-Sánchez, P., Moreno-Chamarro, E., Ortega, P., Blockley, S., Cobb, K. M., Comas-Bru, L., Giralt, S., Goosse, H., Luterbacher, J., Martrat,

B., Muscheler, R., Parnell, A., Pla-Rabes, S., Sjolte, J., Scaife, A. A., Swingedouw, D., Wise, E., & Xu, G. (2020). Modes of climate variability: Synthesis and review of proxy-based reconstructions through the Holocene. *Earth-Science Reviews*, *209*, 103286. https://doi.org/10.1016/j.earscirev.2020.103286

Hersbach, H., Bell, B., Berrisford, P., Biavati, G., Horányi, A., Muñoz Sabater, J., Nicolas, J., Peubey, C., Radu, R., Rozum, I., Schepers, D., Simmons, A., Soci, C., Dee, D., & Thépaut, J.-N. (2018a). ERA5 monthly averaged data on pressure levels from 1979 to present. *Copernicus Climate Change Service (C3S) Climate Data Store (CDS). (Accessed on 01-02-2022)*. https://doi.org/10.24381/cds.6860a573

Hersbach, H., Bell, B., Berrisford, P., Biavati, G., Horányi, A., Muñoz Sabater, J., Nicolas, J., Peubey, C., Radu, R., Rozum, I., Schepers, D., Simmons, A., Soci, C., Dee, D., & Thépaut, J.-N. (2018b). ERA5 monthly averaged data on single levels from 1979 to present. *Copernicus Climate Change Service (C3S) Climate Data Store (CDS). (Accessed on 01-02-2022)*. https://doi.org/10.24381/cds.f17050d7

Hersbach, H., Bell, B., Berrisford, P., Hirahara, S., Horányi, A., Muñoz-Sabater, J., Nicolas, J., Peubey, C., Radu, R., Schepers, D., Simmons, A., Soci, C., Abdalla, S., Abellan, X., Balsamo, G., Bechtold, P., Biavati, G., Bidlot, J., Bonavita, M., ... Thépaut, J.-N. (2020). The ERA5 global reanalysis. *Quarterly Journal of the Royal Meteorological Society*, *146*(730), 1999–2049. https://doi.org/10.1002/qj.3803

Hurrell, J. W. (1995). Decadal Trends in the North Atlantic Oscillation: Regional Temperatures and Precipitation. *Science*, *269*(5224), 676–679. https://doi.org/10.1126/science.269.5224.676

Hurrell, J. W., & Deser, C. (2010). North Atlantic climate variability: The role of the North Atlantic Oscillation. *Journal of Marine Systems*, *79*(3), 231–244. https://doi.org/10.1016/j.jmarsys.2009.11.002

Hurrell, J. W., Kushnir, Y., Ottersen, G., & Visbeck, M. (2003). An Overview of the North Atlantic Oscillation. *The North Atlantic Oscillation: Climatic Significance and Environmental Impact* (pp. 1–35). American Geophysical Union (AGU). https://doi.org/10.1029/134GM01

Hurrell, J. W., & Van Loon, H. (1997). Decadal Variations in Climate Associated with the North Atlantic Oscillation. *Climatic Change*, *36*(3), 301–326. https://doi.org/10.1023/A:1005314315270

IPCC. (2019). *IPCC Special Report on the Ocean and Cryosphere in a Changing Climate* [H.-O. Pörtner, D.C. Roberts, V. Masson-Delmotte, P. Zhai, M. Tignor, E. Poloczanska, K. Mintenbeck, A. Alegría, M. Nicolai, A. Okem, J. Petzold, B. Rama, N.M. Weyer (eds.)]. In press.

Kenyon, J., & Hegerl, G. C. (2008). Influence of Modes of Climate Variability on Global Temperature Extremes. *Journal of Climate*, *21*(15), 3872–3889. https://doi.org/10.1175/2008JCLI2125.1

Lee, J., Sperber, K. R., Gleckler, P. J., Bonfils, C. J. W., & Taylor, K. E. (2019). Quantifying the agreement between observed and simulated extratropical modes of interannual variability. *Climate Dynamics*, *52*(7), 4057–4089. https://doi.org/10.1007/s00382-018-4355-4

Lehner, F., Raible, C. C., & Stocker, T. F. (2012). Testing the robustness of a precipitation proxy-based North Atlantic Oscillation reconstruction. *Quaternary Science Reviews*, *45*, 85–94. https://doi.org/10.1016/j.quascirev.2012.04.025

Lorenz, E. N. (1956). *Empirical Orthogonal Functions and Statistical Weather Prediction* (Sci. Rep. No. 1, Statistical Forecasting Project). M.I.T. Cambridge, MA. http://www.o3d.org/abracco/Atlantic/Lorenz1956.pdf

Lu, J., & Greatbatch, R. J. (2002). The changing relationship between the NAO and northern hemisphere climate variability. *Geophysical Research Letters*, *29*(7), 52–1–52–4. https://doi.org/10.1029/2001GL014052

Mann, M. E., Steinman, B. A., & Miller, S. K. (2020). Absence of internal multidecadal and interdecadal oscillations in climate model simulations. *Nature Communications*, *11*(1), 49. https://doi.org/10.1038/s41467-019-13823-w

Mitchell, J. M. (1976). An Overview of Climatic Variability and its Causal Mechanisms [Edition: 2017/01/20 Publisher: Cambridge University Press]. *Quaternary Research*, *6*(4), 481–493. https://doi.org/10.1016/0033-5894(76)90021-1

Neukom, R., Barboza, L. A., Erb, M. P., Shi, F., Emile-Geay, J., Evans, M. N., Franke, J., Kaufman, D. S., Lücke, L., Rehfeld, K., Schurer, A., Zhu, F., Brönnimann, S., Hakim, G. J., Henley, B. J., Ljungqvist, F. C., McKay, N., Valler, V., von Gunten, L., & PAGES 2k Consortium. (2019). Consistent multidecadal variability in global temperature reconstructions and simulations over the Common Era. *Nature Geoscience*, *12*(8), 643–649. https://doi.org/10.1038/s41561-019-0400-0

North, G. R., Bell, T. L., Cahalan, R. F., & Moeng, F. J. (1982). Sampling errors in the estimation of empirical orthogonal functions. *Monthly Weather Review*, *110*(7), 699–706. https://doi.org/10.1175/1520-0493(1982)110⟨0699:SEITEO⟩2.0.CO;2

Ortega, P., Lehner, F., Swingedouw, D., Masson-Delmotte, V., Raible, C. C., Casado, M., & Yiou, P. (2015). A model-tested North Atlantic Oscillation reconstruction for the past millennium. *Nature*, *523*(7558), 71–74. https://doi.org/10.1038/nature14518

Payton, M. E., Greenstone, M. H., & Schenker, N. (2003). Overlapping confidence intervals or standard error intervals: What do they mean in terms of statistical significance? *Journal of insect science (Online)*, *3*, 34–34. https://doi.org/10.1093/jis/3.1.34

Rahmstorf, S., Box, J. E., Feulner, G., Mann, M. E., Robinson, A., Rutherford, S., & Schaffernicht, E. J. (2015). Exceptional twentieth-century slowdown in Atlantic Ocean overturning circulation. *Nature Climate Change*, *5*(5), 475–480. https://doi.org/10.1038/nclimate2554

Ruggieri, P., Alvarez-Castro, M. C., Athanasiadis, P., Bellucci, A., Materia, S., & Gualdi, S. (2020). North Atlantic Circulation Regimes and Heat Transport by Synoptic Eddies. *Journal of Climate*, *33*(11), 4769–4785. https://doi.org/10.1175/JCLI-D-19-0498.1

Schmith, T., Olsen, S. M., Yang, S., & Christensen, J. H. (2022). *Asymmetries in Circulation Anomalies related to the Phases of the North Atlantic Oscillation on Synoptic Time Scales.*

Schulzweida, U. (2021). CDO User Guide (Version 2.0.0). *Zenodo*. http://doi.org/10.5281/zenodo.5614769

Shabbar, A., Huang, J., & Higuchi, K. (2001). The relationship between the wintertime north Atlantic oscillation and blocking episodes in the north Atlantic. *International Journal of Climatology*, *21*(3), 355–369. https://doi.org/10.1002/joc.612

Smith, D. M., Scaife, A. A., Eade, R., Athanasiadis, P., Bellucci, A., Bethke, I., Bilbao, R., Borchert, L. F., Caron, L.-P., Counillon, F., Danabasoglu, G., Delworth, T., Doblas-Reyes, F. J., Dunstone, N. J., Estella-Perez, V., Flavoni, S., Hermanson, L., Keenlyside, N., Kharin, V., ... Zhang, L. (2020). North Atlantic climate far more predictable than models imply. *Nature*, *583*(7818), 796–800. https://doi.org/10.1038/s41586-020-2525-0

Stephenson, D. B., Hannachi, A., & O'Neill, A. (2004). On the existence of multiple climate regimes. *Quarterly Journal of the Royal Meteorological Society*, *130*(597), 583–605. https://doi.org/10.1256/qj.02.146

Trigo, R. M., García-Herrera, R., Díaz, J., Trigo, I. F., & Valente, M. A. (2005). How exceptional was the early August 2003 heatwave in France? *Geophysical Research Letters*, *32*(10). https://doi.org/10.1029/2005GL022410

Vinther, B. M., Johnsen, S. J., Andersen, K. K., Clausen, H. B., & Hansen, A. W. (2003). NAO signal recorded in the stable isotopes of Greenland ice cores. *Geophysical Research Letters*, *30*(7). https://doi.org/10.1029/2002GL016193

Wanner, H., Brönnimann, S., Casty, C., Gyalistras, D., Luterbacher, J., Schmutz, C., Stephenson, D. B., & Xoplaki, E. (2001). North Atlantic Oscillation – Concepts And Studies. *Surveys in Geophysics*, *22*(4), 321–381. https://doi.org/10.1023/A:1014217317898

Woollings, T., Gregory, J. M., Pinto, J. G., Reyers, M., & Brayshaw, D. J. (2012). Response of the North Atlantic storm track to climate change shaped by ocean–atmosphere coupling. *Nature Geoscience*, *5*(5), 313–317. https://doi.org/10.1038/ngeo1438

Appendix

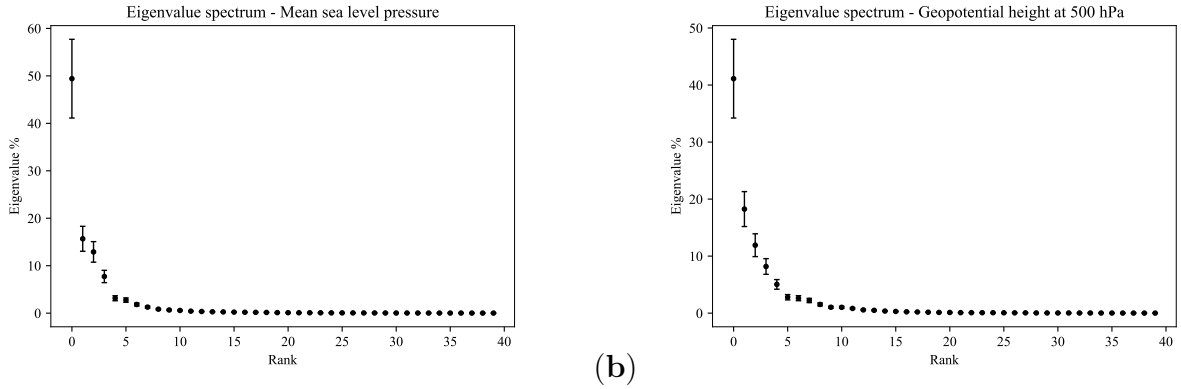

(a) (b)

Figure A.1: Eigenvalue spectrum, in percentage, of the covariance matrix of the *extended winter season* of (a) *MSLP* and (b) *GP500* for the North Atlantic region. Vertical bars show approximate 95 % confidence limits given by the rule of thumb (equation 7). The leading 40 eigenvalues are shown.

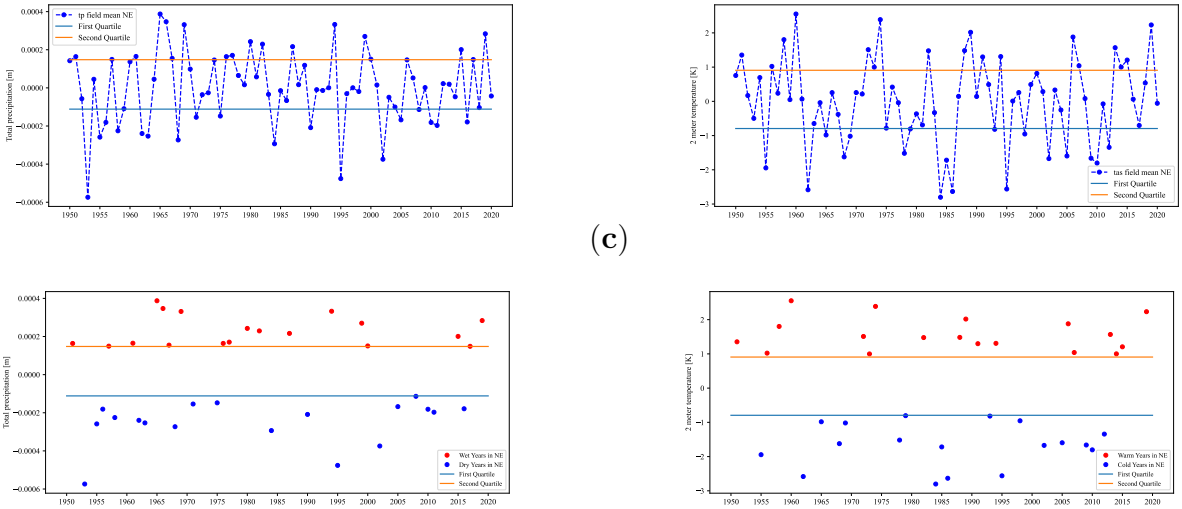

(a) (c)

(d) (d)

Figure A.2: (a), (c) precipitation and (b), (d) temperature quartiles of the Northern European domain (45-75°N/10°W-40°E).

Table A.1: Explained variance of the different analyzed timeseries for all four leading *EOFs* and per defined mode of variability. Following abbreviations are not yet defined: *five-year running mean* period = *5YRM*, *Eastern Atlantic* pattern = *EA*, *Northern European* pattern = *WA*, *Western European* pattern = *WA*

	Total	NAO	WA	NE	WE
GP500	79.5 %	41.1 %	18.3 %	11.9 %	8.2 %
MSLP	85.7 %	49.4 %	15.7 %	12.9 %	7.7 %
5YRM	88.7 %	61.1 %	13.2 %	5.6 % (EOF4)	8.8 % (EOF3)
Cold	85.7 %	46.2 %	13.7 % (EOF3)	20.4 % (EOF2)	5.3 %
Warm	81.8 %	18.4 % (EOF3)	31.1 % (EOF1)	23.3 % (EOF2)	8.8 %
Dry	89.2 %	59.2 %	15.9 %	6.4 % (EOF4)	7.7 % (EOF3)
Wet	88.2 %	56.0 %	20.1 %	5.5 % (EOF4)	6.6 % (EOF3)

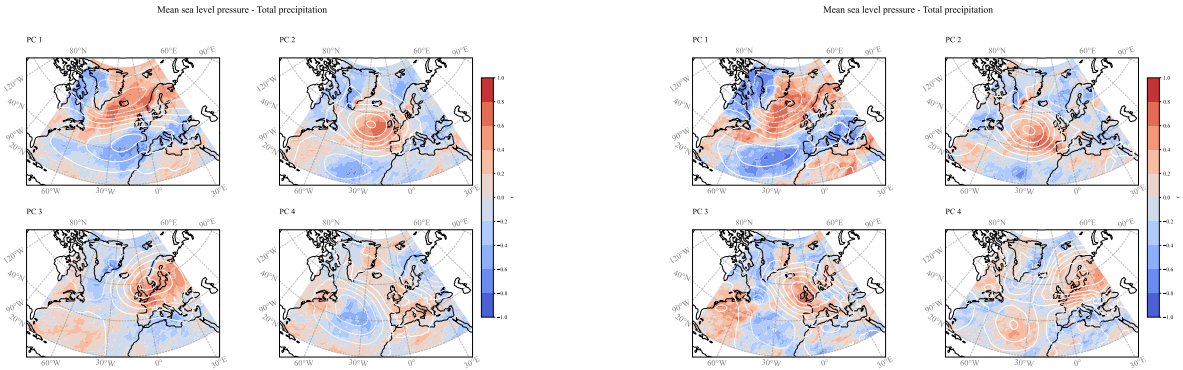

(a) (c)

Figure A.3: Correlation maps of *MSLP* and total precipitation anomalies for the (a) extended winter seasonal mean and (b) the *five-year running mean* of the extended winter season in the North Atlantic region for the period 1950-2021. White contour lines indicate the respective *EOF* pattern with negative values in dashed and positive in solid lines.

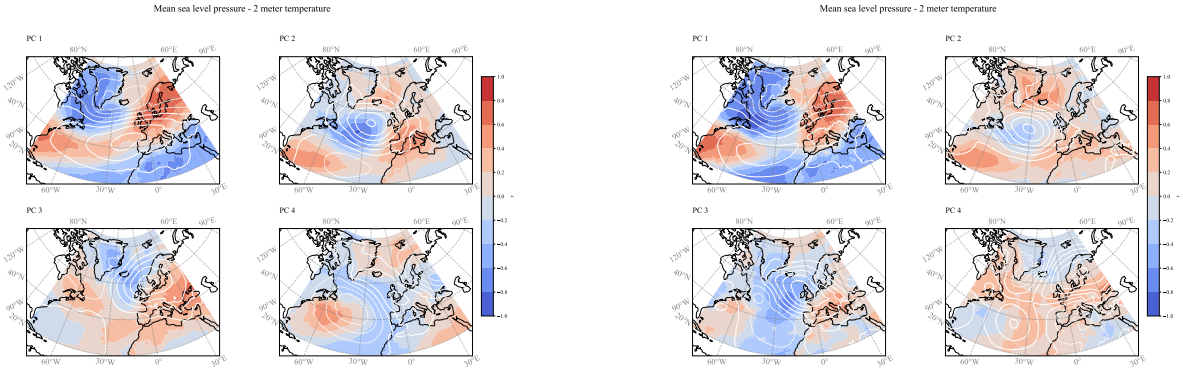

(a) (c)

Figure A.4: Correlation maps of *MSLP* and two-meter temperature anomalies for the (a) extended winter seasonal mean and (b) the *five-year running mean* of the extended winter season in the North Atlantic region for the period 1950-2021. White contour lines indicate the respective *EOF* pattern with negative values in dashed and positive in solid lines.

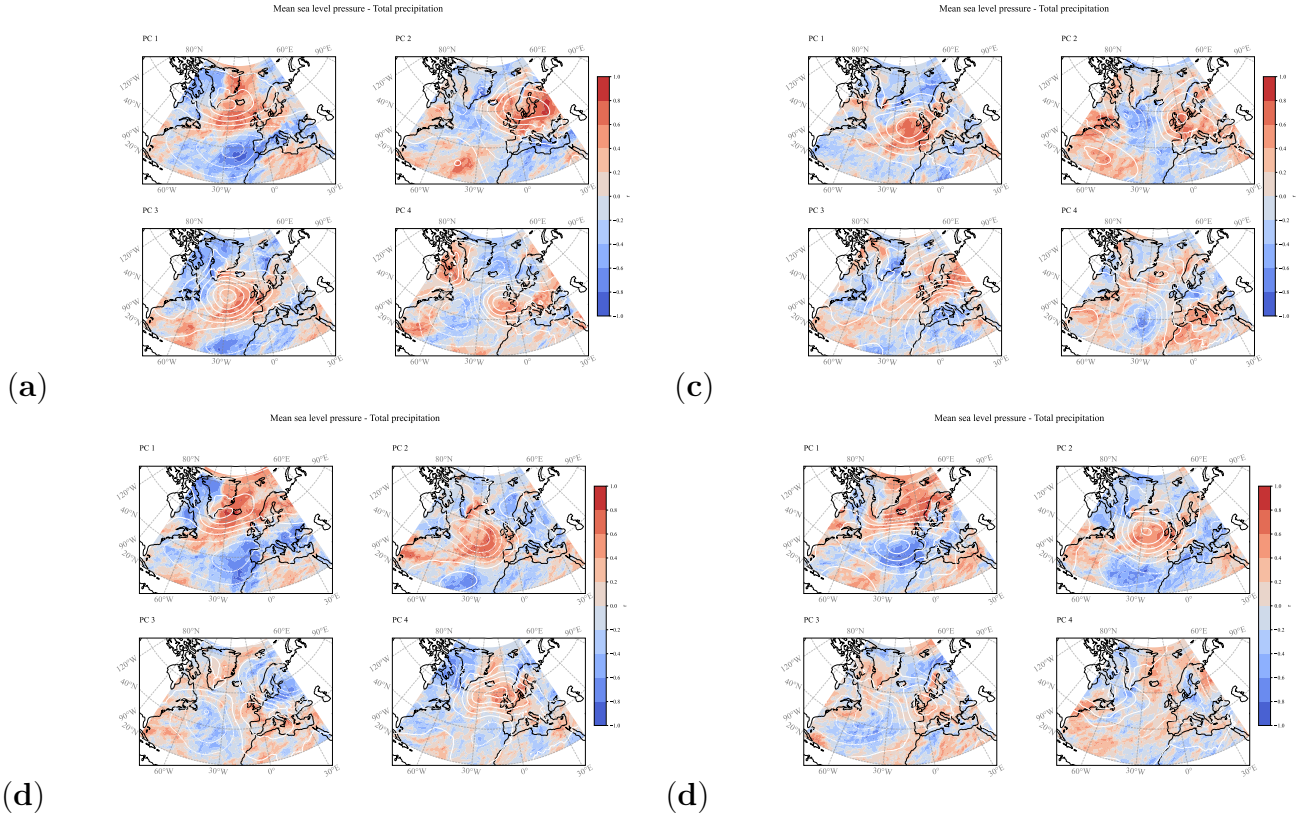

Figure A.5: Correlation maps of *MSLP* and total precipitation anomalies in the North Atlantic region calculated for the (a) cold, (b) warm, (c) dry, and (d) wet quartiles of the Northern European domain over the period 1950-2021. White contour lines indicate the respective *EOF* pattern with negative values in dashed and positive in solid lines.

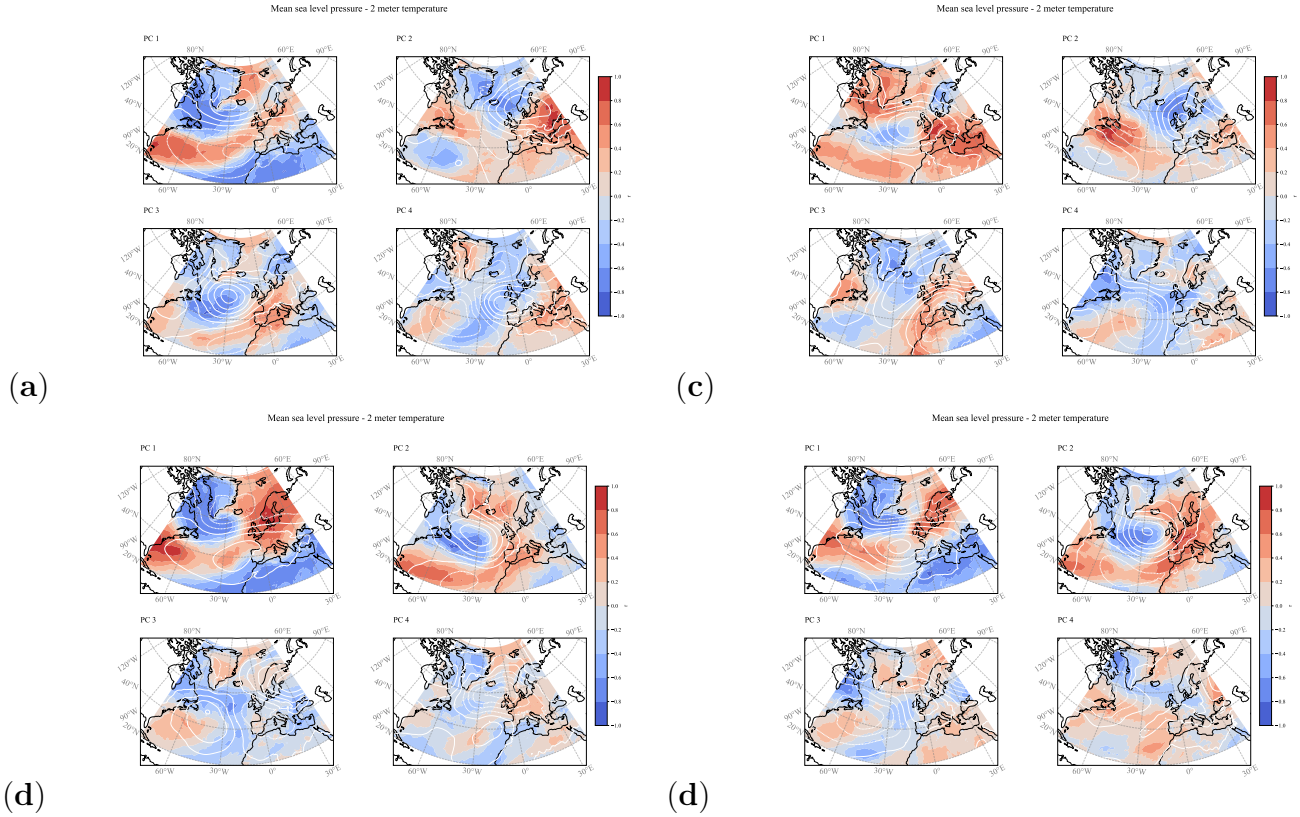

Figure A.6: Correlation maps of *MSLP* and two-meter temperature anomalies in the North Atlantic region calculated for the (a) cold, (b) warm, (c) dry, and (d) wet quartiles of the Northern European domain over the period 1950-2021. White contour lines indicate the respective *EOF* pattern with negative values in dashed and positive in solid lines.